

TRANSFER LEARNING FOR ROBOTICS:
CAN A ROBOT LEARN FROM ANOTHER ROBOT'S DATA?

by

Kaizad V. Raimalwala

A thesis submitted in conformity with the requirements
for the degree of Master of Applied Science
Graduate Department of Aerospace Science and Engineering
University of Toronto

© Copyright 2015 by Kaizad V. Raimalwala

Abstract

Transfer Learning for Robotics:
Can a Robot Learn from Another Robot's Data?

Kaizad V. Raimalwala

Master of Applied Science

Graduate Department of Aerospace Science and Engineering

University of Toronto

2015

Machine learning methods have been used to improve the performance of control systems with experimental data when accurate system or environment models are unavailable. Transfer Learning (TL) allows for this data to come from another, similar system. A simplified TL scenario is studied to understand how the quality of an alignment-based transfer of data varies with the parameters of two linear, time-invariant (LTI), single-input, single-output systems that are tasked to follow the same reference signal. A scalar, LTI transformation is used to align the output from a source system to the output from a target system. An upper bound on the 2-norm of the transformation error is derived and minimized with respect to the transformation scalar. This minimized bound is analyzed with respect to the system parameters to show when TL works best. TL is further studied for wheeled robots, with data from simulation and experiment to supplement theoretical analysis.

In this thesis, condensed versions of Chapters 1, 2, 3, and 4.1 have been published in the proceedings of the 2015 IEEE/RSJ International Conference on Intelligent Robots and Systems (IROS) [13]. The remainder of this thesis contains unpublished material.

Acknowledgements

In the past two years, I have begun my career in robotics through a fantastic Master’s program at the University of Toronto Institute for Aerospace Studies (UTIAS). I could not have asked for a better opportunity and I thank my supervisor Prof. Angela Schoellig for it. Her guidance, encouragement, and commitment to high-quality research have been instrumental in shaping my early professional development and raising my standard of critical thinking, reading and writing. I also thank Prof. Bruce Francis for contributing key ideas to this project, for providing financial support, and most importantly, for teaching me to be attentive to mathematical detail and style of writing.

At UTIAS, I have had the pleasure of meeting some great people. Thank you to my colleagues at DSL and STARS, Chris, Karime, Rikky, Thanh, Lee, Valentin, and Jacob for making my two years here memorable, and to Charlie, Adrian, and Yilun, who helped me with my experimental work. Thank you also to Felix Berkenkamp for giving me great feedback on my work, to Prof. Chris Damaren for reviewing my thesis, and to Prof. Timothy Barfoot and Prof. Gabriel D’Eleuterio for their feedback on my early work.

At Purdue University, I had an excellent four years of undergraduate study and I thank Prof. Daniel DeLaurentis and Prof. Alina Alexeenko for giving my first experiences in an academic research environment. I would be remiss if I also did not thank Jonathan Bunyan, my roommate for four years, whose work ethic and high standards challenged me to improve myself further, and Ms. Priti Suresh, my high-school physics teacher, who nurtured my early predisposition to science.

To my partner Bushra Ilyas, I thank you for your understanding and support through the ups and downs of this amazing journey. Lastly, I thank my parents Roshni and Viraf Raimalwala, and my brother Arzan, whose support and encouragement have made it possible for me to flourish as an individual and pursue my dreams.

“Somewhere, something incredible is waiting to be known.”

– Carl Sagan

Contents

1	Introduction	1
2	Background	4
2.1	Model Learning	4
2.2	Transfer Learning	5
3	Output Transfer – A Bound on the Transfer Error 2-Norm	7
3.1	Problem Formulation	7
3.2	Analysis of the Error Bound	9
4	Extensions to the Output Transfer Case	15
4.1	Input–Output Transfer Case	15
4.2	Output Transfer Case – With Low-Pass Filter	18
4.3	Output Transfer Case – Pole Uncertainty	20
4.3.1	Adding Uncertainty to One System	21
4.3.2	Adding Uncertainty to the Transfer System	23
4.4	Summary of Theoretical Results	25
5	Transfer Learning for 2D Wheeled Robots	27
5.1	Kinematic Model and Linearization about a Point Ahead	28
5.2	Analysis of the Bound on the Transfer Error 2-Norm	30
5.3	Alignment–based Transfer Learning with Simulation Data	32
5.4	Alignment–based Transfer Learning with Experimental Data	37
5.5	Summary	40

6	Conclusions and Outlook	41
A	Proof for Lemma 1	44
B	Proof for Theorem 1	50
C	Roots of the Biquadratic Equation	52
	Bibliography	54

List of Tables

5.3.1 The 2-norm of the 1D and 2D transformation errors and of the difference between the source and target trajectories.	34
5.4.1 A table of $\ e_A\ _2$ for different gain combinations used in the Pioneer experiment.	40

List of Figures

1.0.1 Transfer Learning framework.	2
3.1.1 Control Block Diagram: Output Transfer (OT) case.	8
3.2.1 Contour plot of error bound in OT case (left). Contour plot of error bound in OT case with constant DC gain (right).	13
4.1.1 Control Block Diagram: Input-Output Transfer (IOT) case.	16
4.1.2 Contour plot of error bound in IOT case (left). Contour plot of ratio of error bound in IOT case to that in OT case (right).	18
4.2.1 Control Block Diagram: Output Transfer case with low-pass filter (OT- LPF) (left). Effect of a low-pass filter (right)	19
4.2.2 Contour plot of error bound in OT-LPF case (left). Contour plot of error bound in OT-LPF case with constant DC gain (right).	20
4.3.1 Control Block Diagram: System with inverse multiplicative uncertainty added.	21
4.3.2 Control Block Diagram: OT case with pole uncertainty (OT-UNC) . . .	23
4.3.3 Contour plot of error bound in OT-UNC case (left). Contour plot of error bound in OT-UNC case with constant DC gain (right).	25
5.1.1 Unicycle in 2D plane (left) and linearized unicycle in complex plane (right). 29	
5.1.2 2D decomposition of linearized unicycle system with proportional feedback control.	30
5.3.1 In simulation: two unicycle robots move in spiral path (left). Transfer error plots (right).	35

5.3.2 Contour plot of 1D transfer error 2-norm for unicycle robots in simulation (left). Contour plot of ratio of 2D to 1D transfer error 2-norms (right).	36
5.3.3 Line plots (cross-sections of transfer error contour plots) for linearized unicycle (left), nonlinear unicycle (centre) and OT-LPF with constant DC gain (right).	37
5.4.1 In experiment: The Pioneer 3A-T robot (left). Two spiral trajectories and alignments (right).	38
5.4.2 In experiment: Transfer error plots.	39
6.0.1 A summary of the tools used to study TL in this project.	42

Chapter 1

Introduction

Models that accurately represent dynamic systems are often difficult to derive mathematically, or are unreliable due to parameter uncertainties or unknown external disturbances affecting the system. The potential use of data from simulations or experiments to improve models of dynamic systems is a prime motivator for modern research at the intersection of machine learning and control theory. Various regression techniques have been used to learn dynamics, kinematics and disturbance models using data from physical trials or simulations of the robot [2, 10, 12, 16].

Transfer Learning (TL) allows for this data to be generated by a second system. In a training phase, both systems generate data, and a transformation that aligns one dataset to the other is learned. Once this mapping is learned, the first system, also called the target system, can use data generated by the second system, the source system, in subsequent model learning (see Fig. 1.0.1). This transfer of data may be beneficial to the model learning process if the source system is less costly, difficult, or hazardous to operate than the target system.

In this paper, we study when such a data transfer is beneficial. We investigate TL for two simple, linear, time-invariant (LTI), single-input, single-output (SISO) systems. We use an H_∞ -norm minimization framework to define the quality of the data transfer and analyze when the transfer works well and when it does not.

In robotics, TL has often been considered in the context of speeding up a single robot's task learning using knowledge obtained in a previous task performed by the same

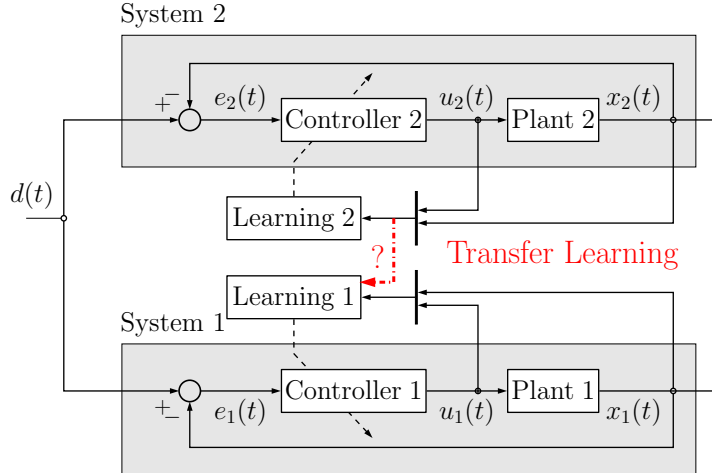


Figure 1.0.1: Transfer Learning framework. Systems 1 and 2 learn from input-output data (dashed lines). The concept of Transfer Learning (TL) allows for System 1 to use data from System 2 for its own learning task (red dash-dotted line). In this paper, we study TL from a system-theoretic perspective and provide insight to when TL is beneficial.

robot. TL has, for example, been successfully used in an Iterative Learning Control (ILC) framework to speed up learning of new tasks [1, 7, 8]. Research for multi-agent robotic systems is relatively sparse [19]. Most common applications aim to speed up joint or sequential learning either in an ILC framework by transferring task-dependent disturbance estimates [15], or in a Reinforcement Learning framework by transferring rules and policies of simple systems with discrete states [4, 9, 18]. However, TL can also be used in a model learning framework to apply a transformation on input-output data generated by one robot. This transformed data can then be input to a model learning algorithm for a second, similar robot [3]. We are interested in the latter multi-agent learning scenario.

In several applications beyond robotics, Manifold Alignment has been used to find an optimal transformation to align datasets [6, 21]. In [20], this technique is demonstrated for two simple state-space models that each need to learn a task using Reinforcement Learning. In [3], a similar transformation technique is used on data from one robotic arm to speed up learning of a robot model for a second robotic arm.

While these works have shown that TL is feasible for some examples, they do not address the question of when the data transfer works well and when it fails. This paper provides insight on how the quality of the transformation depends on the system proper-

ties of the source and target systems. We study two first-order, LTI, SISO systems tasked to follow the same reference signal and show that the transfer quality depends on the location of the poles (that is, the stability properties) of both systems. Furthermore, to the best of the authors' knowledge, TL between two mobile robots has not been studied, either in simulation, or in practice.

Despite the simplicity of the systems we choose to study, this paper offers two novel results. Firstly, we study the feasibility of TL for control systems from a system-theoretic perspective by formulating the problem as an H_∞ -norm minimization problem. An upper bound on the 2-norm of the transformation error for a large set of reference signals is derived and minimized with respect to the transformation parameter. We then analyze how this minimized upper bound depends on the parameters of the two systems, namely the poles and the gains. From this analysis, we can gain insight for which configurations TL works best in this simplified scenario. We then consider how these results change when the reference signal is used as an additional input to the transformation. To further extend this analysis, we study two more cases: (i) when the two systems are tasked to follow a reference signal from a smaller, more realistic set, and (ii) when the two systems have uncertain poles.

Secondly, we analyze TL for two wheeled robots in three ways: (i) using the H_∞ -norm minimization framework for systems represented by linearized kinematic unicycle models, (ii) using data generated in simulation of the linearized and nonlinear kinematic models, and (iii) with experimental data from a Pioneer robot.

The remainder of the thesis is structured as follows: Chapter 2 provides a background on model learning and TL for control systems. In Chapter 3, the problem of TL for the two first-order, LTI, SISO systems is presented and the minimized upper bound on the 2-norm of the transformation error is derived. In Chapter 4, further results are derived for the extension problems and analyzed. In Chapter 5, TL is studied for two wheeled robots as previously mentioned. Lastly, Chapter 6 provides concluding remarks.

Chapter 2

Background

2.1 Model Learning

Dynamics and kinematics models govern a robot's behavior. While analytic models can be derived from first principles, they often do not capture the real-world dynamics accurately [2, 12]. Supervised model learning presents a solution by employing a regression tool to find a map from input data to labelled observations. Given a sequence of input-output data with input $\mathbf{x}[k] \in \mathbb{R}^n$ and output $\mathbf{y}[k] \in \mathbb{R}^p$, where $k \in \{0, 1, 2, \dots, N\}$ and N is the number of samples obtained, the problem of model learning is to find a map $\mathcal{M} : \mathbf{f}(\mathbf{x}) \rightarrow \mathbf{y}$ such that some measure of the magnitude of the error sequence,

$$\boldsymbol{\epsilon}[k] = \mathbf{y}[k] - \mathbf{f}(\mathbf{x}[k]), \quad k \in \{0, 1, 2, \dots, N\}, \quad (2.1.1)$$

is minimized. For example, learning an inverse dynamics model for a robot arm can be formulated as finding a map $\mathcal{M} : \mathbf{f}(\mathbf{q}, \dot{\mathbf{q}}, \ddot{\mathbf{q}}) \rightarrow \boldsymbol{\tau}$, where $\mathbf{q} \in \mathbb{R}^p$ is a vector of joint angles for all p joints of the arm, $\boldsymbol{\tau} \in \mathbb{R}^p$ is a vector of applied torques to each joint and $\mathbf{x} \in \mathbb{R}^{3p}$ [11].

2.2 Transfer Learning

When two robots (or control systems, in general) S_1 and S_2 execute a task, data is generated by each system. Data from S_2 can then undergo a transformation to align with data from S_1 . The problem is akin to model learning in that a map needs to be found. In [3] and [20], the authors model this map as an LTI transformation for each data sample. We make the same assumption.

Let vectors $\mathbf{x}_1[k]$ and $\mathbf{x}_2[k]$ be sampled data from S_1 and S_2 . We thus define the problem of TL as finding a matrix \mathbf{A} such that the vector 2-norm of

$$\boldsymbol{\epsilon}[k] = \mathbf{x}_1[k] - \mathbf{A}\mathbf{x}_2[k] \quad (2.2.1)$$

is minimized for all times $k \in \{0, 1, 2, \dots, N\}$. The vector \mathbf{x} can consist of system states, control inputs, or other variables that are relevant for a specific model learning algorithm. For the inverse dynamics model learning example in [3], the vector \mathbf{x} is defined as $\mathbf{x} = [\mathbf{q}^T, \dot{\mathbf{q}}^T, \ddot{\mathbf{q}}^T, \mathbf{u}^T]^T$. Once such a matrix is learned from one pair of datasets, additional training data for learning the model of S_1 can be obtained by transforming subsequent data collected from S_2 using \mathbf{A} .

To find an optimal transformation that aligns the discrete datasets, *a priori* models of each system need not be known, as the transformation only depends on data collected from physical trials of the two systems. The disadvantage of this data-alignment technique is that it is difficult to make predictions on the quality of the transformation. Furthermore, there usually is no guarantee on the performance of a given transformation on subsequent data.

Work in [3] shows that for two simulated robot arms, the data alignment worked well and sped up model learning. However, it is not obvious that the same approach works in other applications. Our work is motivated by an interest to further explore the properties of an LTI transformation for control system data, and determine when TL is most beneficial and when it fails.

We therefore choose to study two first-order, LTI, SISO systems, S_1 and S_2 . In this framework, $\mathbf{x}_1(t) = x_1(t)$, and $\mathbf{x}_2(t) = x_2(t)$ are the scalar states of both systems

and $\mathbf{A} = \alpha$ is a scalar that must map $x_2(t)$ to $x_1(t)$. For reference signals in the set $\mathcal{D} = \{d(t) : \|d\|_2 \leq 1\}$, a unique α^* is found to optimally align $x_2(t)$ to $x_1(t)$ for all $t \in [0, \infty)$ in an H_∞ -norm sense. We call this approach the Output Transfer (OT) case.

In a second scenario, which we call the Input-Output Transfer (IOT) case, we study the case when the common reference signal $d(t)$ is used in the transformation; that is, $\mathbf{x}_2(t) = [x_2(t), d(t)]^T$ and $\mathbf{A} = [\beta_1, \beta_2]$. A transformation $\{\beta_1^*, \beta_2^*\}$ is numerically found to optimally align a linear combination of $x_2(t)$ and $d(t)$ to $x_1(t)$ for all $t \in [0, \infty)$ in an H_∞ -norm sense.

In both cases, we derive an upper bound on the 2-norm of the transformation error signal and minimize it with respect to the transformation parameters. We show that for these simple systems, the minimized upper bound strongly depends on the poles of S_1 and S_2 , and that systems with a fast response have an advantage over systems with a slow response. We further show that the IOT case reduces the minimized error bound.

In the OT case, we extend our analysis in two ways. In the first, we add a low-pass filter to filter out high-frequency components of the reference signals in \mathcal{D} . This allows us to study how the quality of TL varies the system parameters for more realistic reference signals. In the second, we study what happens when the two systems have uncertain poles. This provides some initial insight into the problem of TL when the two systems are not completely known, for example, robots that need to learn part of their models.

Lastly, we demonstrate the data-alignment technique for two unicycle models and compare how the transformation error computed from data generated in simulation by a specific reference signal varies with source and target system parameters to the variation of the minimized error bound found through our mathematical analysis for the set \mathcal{D} .

Chapter 3

Output Transfer – A Bound on the Transfer Error 2-Norm

3.1 Problem Formulation

In this section, we introduce a framework for analyzing TL for simple, LTI, SISO systems and define the H_∞ -norm minimization problem for the OT case; that is, the case where a scalar α is used to align $x_2(t)$, the output of the source system, to $x_1(t)$, the output of the target system.

These two systems have transfer functions

$$G_1(s) = \frac{k_1}{s + a_1}, \quad (3.1.1)$$

$$G_2(s) = \frac{k_2}{s + a_2}, \quad (3.1.2)$$

where $-a_1$ and $-a_2$ are the poles, and k_1 and k_2 are the gains of G_1 and G_2 (see Fig. 3.1.1). These transfer functions can represent path-following robots with closed-loop poles $-a_1$ and $-a_2$ and proportional feedback controller gains k_1 and k_2 . For example, a unicycle's linearized kinematics model with proportional feedback control with gain k can be represented by the transfer function $k(s + k)^{-1}$ (see Section 5.1).

The quantity of interest in the TL problem for the OT case is the error of the alignment

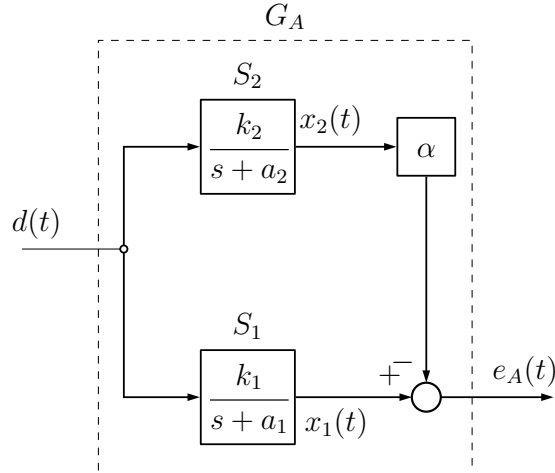


Figure 3.1.1: In the Output Transfer case, the signal $x_2(t)$ is weighted by a scalar α to match $x_1(t)$. While $x_1(t)$ and $x_2(t)$ are outputs of sub-systems S_1 and S_2 , the output of the overall system is $e_A(t)$.

of $x_2(t)$ to $x_1(t)$ and is the output of the transfer system,

$$e_A(t) = x_1(t) - \alpha x_2(t), \quad (3.1.3)$$

where α is a time-invariant scalar. The transfer function from $d(t)$ to $e_A(t)$ is

$$G_A(s) = \frac{k_1}{s + a_1} - \alpha \frac{k_2}{s + a_2}. \quad (3.1.4)$$

To assure that $G_A(s)$ is asymptotically stable, a_1 and a_2 are assumed to be positive. Furthermore, k_2 is assumed to be non-zero to avoid the degenerate case where $G_A = G_1$.

Design Criterion. The signal 2-norm is chosen as a measure for the signals $e_A(t)$ and is denoted by $\|\cdot\|_2$. This measure can be determined for a specific reference signal $d(t) \in \mathcal{L}_2[0, \infty)$, where $\mathcal{L}_2[0, \infty)$ denotes the set of all signals that have finite energy on an infinite time interval $[0, \infty)$. However, the H_∞ -norm of G_A provides the least upper bound on $\|e_A\|_2$ for all $d(t) \in \mathcal{D}$, as shown in [5]; that is,

$$\|G_A\|_\infty = \sup\{\|e_A\|_2 : d(t) \in \mathcal{D}\}, \quad (3.1.5)$$

the H_∞ -norm of G_A is defined as

$$\|G_A\|_\infty := \sup_{\omega} |G_A(j\omega, \alpha)|. \quad (3.1.6)$$

Definition 1. *The transfer problem is formulated as minimizing $\|G_A\|_\infty$ with respect to α :*

$$\alpha^* := \arg \min_{\alpha} \|G_A\|_\infty. \quad (3.1.7)$$

The H_∞ -norm is useful in analyzing the properties of TL for a large set of reference signals. Assuming that any signal in \mathcal{D} is a potential reference signal, the optimal transformation α^* represents the best possible transformation that would be obtained when observing the system for an infinite amount of time under all possible reference inputs $d(t) \in \mathcal{D}$. Consequently, as long as the reference signal belongs to the set \mathcal{D} , the H_∞ -norm evaluated at α^* provides the worst possible transformation error we could get.

3.2 Analysis of the Error Bound

Recall the TL problem for this case,

$$\alpha^* := \arg \min_{\alpha} \|G_A\|_\infty \quad (3.2.1)$$

$$= \arg \min_{\alpha} \|G_A\|_\infty^2, \quad (3.2.2)$$

where minimizing the squared norm with respect to α is the same as minimizing the norm itself. In this section, we derive an analytic expression for $\|G_A\|_\infty^2$ as a function of α , a_1 , a_2 , k_1 , and k_2 , and find $\min_{\alpha} \|G_A\|_\infty^2$ as a function of a_1 , a_2 and k_1 .

To begin, $\|G_A\|_\infty^2$ must be found. It is the peak squared magnitude over all frequencies ω . The squared magnitude of $G_A(j\omega, \alpha)$ is

$$|G_A(j\omega, \alpha)|^2 = \frac{\lambda_1(\alpha)\omega^2 + \lambda_2(\alpha)}{\omega^4 + \lambda_4\omega^2 + \lambda_5}, \quad (3.2.3)$$

where

$$\lambda_1(\alpha) = (k_1 - k_2\alpha)^2, \quad (3.2.4)$$

$$\lambda_2(\alpha) = (k_1a_2 - k_2a_1\alpha)^2, \quad (3.2.5)$$

$$\lambda_4 = a_1^2 + a_2^2, \quad (3.2.6)$$

$$\lambda_5 = a_1^2a_2^2. \quad (3.2.7)$$

The following expressions are used in the subsequent lemma:

$$\alpha_1 = \frac{k_1 a_2}{k_2 a_1^3} (a_1^2 + a_2^2 - a_1 a_2 + \sqrt{(a_1 - a_2)^2 (a_1^2 + a_2^2)}), \quad (3.2.8)$$

$$\alpha_2 = \frac{k_1 a_2}{k_2 a_1^3} (a_1^2 + a_2^2 - a_1 a_2 - \sqrt{(a_1 - a_2)^2 (a_1^2 + a_2^2)}), \quad (3.2.9)$$

$$\phi(\alpha) = \frac{\lambda_1^2}{\lambda_4 \lambda_1 - 2\lambda_2 + 2\sqrt{\lambda_5 \lambda_1^2 - \lambda_4 \lambda_1 \lambda_2 + \lambda_2^2}}, \quad (3.2.10)$$

$$\psi(\alpha) = \frac{\lambda_2(\alpha)}{\lambda_5}. \quad (3.2.11)$$

Lemma 1. For G_A in (3.1.4), $\|G_A\|_\infty^2$ is a piecewise continuous function with respect to α that maximizes $|G_A(j\omega, \alpha)|^2$ in (3.2.3) with respect to ω for all $a_1, a_2 > 0$, k_1 , and $k_2 \neq 0$. With the expressions defined in (3.2.8)-(3.2.11), it is given by

$$\gamma_A^2(\alpha) := \|G_A\|_\infty^2 = \begin{cases} \phi(\alpha) & \text{if } \alpha_2 < \alpha < \alpha_1 \\ \psi(\alpha) & \text{otherwise.} \end{cases} \quad (3.2.12)$$

Proof. The proof is presented in Appendix A. □

The function $\gamma_A^2(\alpha)$ thus provides the least upper bound on $\|e_A\|_2^2$, subject to $d(t) \in \mathcal{D}$, as a function of the user-defined parameter α . This function can be minimized with respect to α . The result is given in Theorem 1.

Theorem 1. For G_A in (3.1.4), the parameter α that minimizes $\|G_A\|_\infty^2$ for

all $a_1, a_2 > 0$, k_1 , and $k_2 \neq 0$ is given by

$$\alpha^* = \frac{k_1}{k_2} \frac{2a_2}{\left(4a_1 + a_2 - \sqrt{8a_1^2 + a_2^2}\right)}. \quad (3.2.13)$$

Proof. The proof is presented in Appendix B. \square

Evaluating $\|G_A\|_\infty^2$ at α^* yields

$$\gamma_A^{*2} := \min_{\alpha} \gamma_A^2(\alpha) \quad (3.2.14)$$

$$= \frac{k_1^2 \left(4a_1^2 - a_2 \left(a_2 + \sqrt{8a_1^2 + a_2^2}\right)\right)^4}{32a_1^2(a_1 + a_2)^3 \left(4a_1a_2\sqrt{\xi_1} + (a_2 - a_1)\xi_2\right)}, \quad (3.2.15)$$

where

$$\xi_1 = 2a_1^2(a_1 - a_2)^2 \left(4a_1^2 + 5a_2^2 - 3a_2\sqrt{8a_1^2 + a_2^2}\right), \quad (3.2.16)$$

$$\xi_2 = a_2^4 - 8a_1^2(a_1^2 + a_2^2) + a_2(4a_1^2 + a_2^2)\sqrt{8a_1^2 + a_2^2}. \quad (3.2.17)$$

Remark 1. If $a_1 = a_2$, the optimization problem in (3.1.7) is trivial; $\alpha^* = k_1k_2^{-1}$ and $\gamma_A^* = 0$. That is, if S_1 and S_2 have identical poles (but potentially different gains), perfect transfer can be achieved with zero transfer error. In this case, α^* only needs to compensate for the difference in the gains of the two systems.

Remark 2. The minimized H_∞ -norm, γ_A^* , is independent of k_2 . This can be explained by observing that in Fig. 3.1.1, insufficient amplification of the output $x_2(t)$, by the gain k_2 , can be compensated by the multiplier α .

Remark 3. If the poles $-a_1$ and $-a_2$ are held constant, γ_A^{*2} is proportional to k_1^2 . As a result, the transfer error decreases if $|k_1|$ is decreased with the degenerate limit case being $k_1 = 0$, $\alpha^* = 0$, $\gamma_A^* = 0$, which achieves perfect matching because the target system outputs zero.

Additionally, the result of Theorem 1 can be analyzed for varying pole combinations $(-a_1, -a_2)$. There are two different ways to interpret the result: (i) by keeping the

target system gain k_1 constant, or (ii) by re-parametrizing the systems using their DC gains $g_1 = k_1 a_1^{-1}$ and $g_2 = k_2 a_2^{-1}$, $G_1 = g_1 a_1 (s + a_1)^{-1}$ and likewise for G_2 , and keeping the DC gains constant.

Corollary 1. *If the target system gain k_1 is held constant, γ_A^* , defined in (3.2.14), approaches infinity as the pole of the target system S_1 approaches the imaginary axis. Therefore, TL may not be beneficial if the target system has a slow response to reference inputs.*

Proof. In (3.2.15), a_1^2 is factored out in the denominator. Therefore, $\lim_{a_1 \rightarrow 0^+} \gamma_A^* \rightarrow \infty$. \square

Corollary 1 shows that TL is problematic if the target system has a pole that is close to the imaginary axis, unless $a_2 \approx a_1$. The interpretation of this is that if $a_1 \ll a_2$, the target system response is slow and does not follow the reference signal well, while the source system does. However, keeping k_1 constant and decreasing a_1 also means that the DC gain g_1 increases, which contributes to the bad transfer quality.

Therefore, it is valuable to study the results under the assumption of constant DC gains, which is more realistic in practice. The minimized bound can then be written as

$$\gamma_A^{*2} = g_1^2 \frac{\left(4a_1^2 - a_2 \left(a_2 + \sqrt{8a_1^2 + a_2^2}\right)\right)^4}{32(a_1 + a_2)^3 \left(4a_1 a_2 \sqrt{\xi_1} + (a_2 - a_1)\xi_2\right)}, \quad (3.2.18)$$

where ξ_1 and ξ_2 are from (3.2.16) and (3.2.17).

Corollary 2. *If g_1 is held constant, it can be shown that $\gamma_A^* \rightarrow |g_1|/4$ as $a_1 \rightarrow 0$ and $\gamma_A^* \rightarrow |g_1|$ as $a_2 \rightarrow 0$.*

Proof. Corollary 2 follows directly from (3.2.16):(3.2.18) by taking the limit $a_1 \rightarrow 0$ and $a_2 \rightarrow 0$. \square

The aforementioned results can be visualized in a contour plot that illustrates how the minimized H_∞ -norm of G_A varies as a function of the pole magnitudes a_1 and a_2 . In Fig. 3.2.1a, we keep k_1 constant (according to Corollary 1). The minimized bound γ_A^* is normalized by $|k_1|$. The base-10 logarithm of the data is shown to illustrate the variation more clearly. A white line is drawn through the diagonal as $\gamma_A^* = 0$ when $a_1 = a_2$.

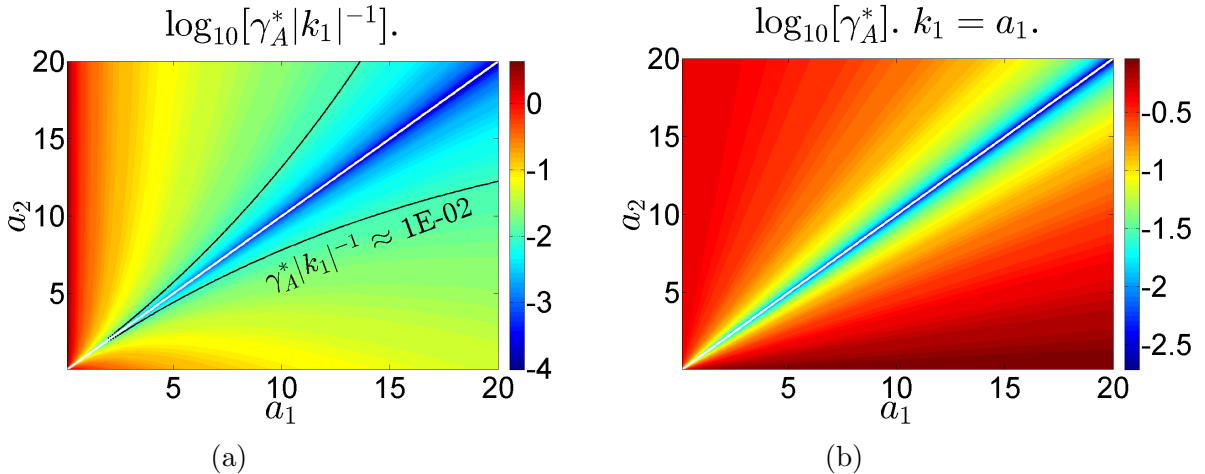


Figure 3.2.1: On the left is a contour plot of $\log_{10}[\gamma_A^*|k_1|^{-1}]$ vs. a_1 and a_2 . When $a_1 = a_2$, $\gamma_A^*|k_1|^{-1}$ is zero. As the pole a_1 approaches zero, $\gamma_A^*|k_1|^{-1}$ grows exponentially. The black line illustrates a constant contour line where $\gamma_A^*|k_1|^{-1} = 1\text{E-}02$. On the right, a contour plot of $\log_{10}[\gamma_A^*]$ vs. a_1 and a_2 is shown for $k_1 = a_1$, that is, $g_1 = 1$.

In Fig. 3.2.1b, a contour plot of γ_A^* is shown, where now the DC gain g_1 is held constant (according to Corollary 2). We chose $g_1 = 1$. This is in contrast to Fig. 3.2.1a where k_1 is held constant.

Key Observation 1: In Fig. 3.2.1a, the minimized H_∞ -norm, γ_A^* , increases exponentially with diminishing a_1 , a result expected from Corollary 1 for constant k_1 . This indicates that S_1 must not have a pole close to the imaginary axis if we want to achieve an accurate data transfer from S_2 to S_1 , unless $|k_1|$ is small as well.

Key Observation 2: For both Figs. 3.2.1a and 3.2.1b with constant k_1 and constant g_1 , respectively, the transfer quality is best if the poles of S_1 and S_2 lie close together.

Key Observation 3: For both Figs. 3.2.1a and 3.2.1b, if the poles a_1 and a_2 are of greater magnitude, they can be further apart for the minimized error bound to stay on the same contour line. For example, consider the two black contour lines for $\gamma_A^*|k_1|^{-1} = 1\text{E-}2$ in Fig. 3.2.1a. If $a_1 = 10$, then to not do worse than an error of around $1\text{E-}2$, a_2 must be approximately between 7.8 and 13.1. However, if $a_1 = 12$, then the range of allowable a_2 increases by around 47% to be approximately between 8.9 and 16.7.

Key Observation 4: According to Fig. 3.2.1b, if the DC gain g_1 is held constant, then it is slightly more preferable to have $a_2 > a_1$, in contrast to if the gain itself, k_1 , is

held constant.

In the next chapter, we extend this analysis to the IOT case, where the reference signal is used in the transformation. We also modify the OT case in two separate ways, one by letting the reference signal go through a low-pass filter, and another by adding uncertainty to the two systems S_1 and S_2 .

Chapter 4

Extensions to the Output Transfer Case

4.1 Input–Output Transfer Case

We now consider the case when the reference signal is also used in the transformation. The output of the transfer system G_B is the error signal

$$e_B(t) = x_1(t) - (\beta_1 x_2(t) + \beta_2 d(t)), \quad (4.1.1)$$

where $\{\beta_1, \beta_2\}$ are time-invariant scalars. This is the Input-Output Transfer case (see Fig. 4.1.1). The transfer function from $d(t)$ to $e_B(t)$ is

$$G_B(s) = \frac{k_1}{s + a_1} - \beta_1 \frac{k_2}{s + a_2} - \beta_2. \quad (4.1.2)$$

Definition 2. *The transfer problem is formulated as minimizing $\|G_B\|_\infty$ with respect to $\{\beta_1, \beta_2\}$:*

$$\{\beta_1^*, \beta_2^*\} := \arg \min_{\{\beta_1, \beta_2\}} \|G_B\|_\infty. \quad (4.1.3)$$

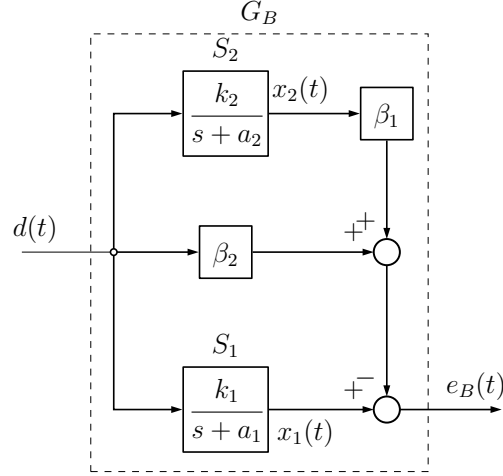


Figure 4.1.1: In the Input-Output Transfer Case, the signal $x_1(t)$ is estimated with a linear combination of $x_2(t)$ and $d(t)$.

Finding equivalent analytic results for the IOT case proved to be more difficult. Results are obtained from numerically finding $\|G_B\|_\infty$ as a function $\boldsymbol{\beta} = [\beta_1, \beta_2]$. Numerical methods can then be used to find an estimate for $\boldsymbol{\beta}^*$, along with $\gamma_B^* := \gamma_B(\boldsymbol{\beta}^*)$, where we use a similar notation as in (3.2.12): $\gamma_B(\boldsymbol{\beta}) := \|G_B\|_\infty$.

The squared magnitude of $G_B(j\omega, \boldsymbol{\beta})$ is

$$|G_B(j\omega, \boldsymbol{\beta})|^2 = \frac{\theta_1(\boldsymbol{\beta})\omega^4 + \theta_2(\boldsymbol{\beta})\omega^2 + \theta_3(\boldsymbol{\beta})}{\omega^4 + \lambda_4\omega^2 + \lambda_5}, \quad (4.1.4)$$

where

$$\theta_1(\boldsymbol{\beta}) = \beta_2^2, \quad (4.1.5)$$

$$\theta_2(\boldsymbol{\beta}) = (k_2\beta_1 + a_2\beta_2)^2 + (k_1 - a_1\beta_2)^2 - 2\beta_1k_1k_2, \quad (4.1.6)$$

$$\theta_3(\boldsymbol{\beta}) = (a_1(k_2\beta_1 + a_2\beta_2) - a_2k_1)^2. \quad (4.1.7)$$

After finding the roots of the partial derivative of $|G_B(j\omega, \boldsymbol{\beta})|^2$ with respect to ω , it can be shown that

$$\gamma_B^2(\boldsymbol{\beta}) = \max \left(\beta_2^2, \frac{\theta_3(\boldsymbol{\beta})}{\lambda_4}, |G_B(j\omega_2, \boldsymbol{\beta})|^2 \right), \quad (4.1.8)$$

where

$$\omega_2^2 = 2\sqrt{p(\boldsymbol{\beta})^2 - q(\boldsymbol{\beta})} - 2p(\boldsymbol{\beta}), \quad (4.1.9)$$

$$p(\boldsymbol{\beta}) = \frac{1}{2} \frac{\lambda_5 \theta_1(\boldsymbol{\beta}) - \theta_3(\boldsymbol{\beta})}{\lambda_4 \theta_1(\boldsymbol{\beta}) - \theta_2(\boldsymbol{\beta})}, \quad (4.1.10)$$

$$q(\boldsymbol{\beta}) = \frac{1}{4} \frac{\lambda_5 \theta_2(\boldsymbol{\beta}) - \lambda_4 \theta_3(\boldsymbol{\beta})}{\lambda_4 \theta_1(\boldsymbol{\beta}) - \theta_2(\boldsymbol{\beta})}. \quad (4.1.11)$$

Remark 4. *If $a_1 = a_2$, the optimization problem in (4.1.3) is trivial: $\boldsymbol{\beta}^* = [k_1 k_2^{-1}, 0]$ and $\gamma_B^* = 0$.*

In Fig. 4.1.2a, a contour plot illustrates how the minimized H_∞ -norm of G_B varies as a function of the pole magnitudes a_1 and a_2 . To compare the minimized H_∞ -norms of the transfer functions G_A and G_B , a contour plot of the ratio γ_B^*/γ_A^* is shown in Fig. 4.1.2b. This ratio is undefined when $a_1 = a_2$ because $\gamma_A^* = \gamma_B^* = 0$. For γ_B^* , no closed-form solutions are available to suggest how γ_B^* may be normalized, if at all. Therefore, k_1 and k_2 are both set to one in Figs. 4.1.2a and 4.1.2b. To obtain $\boldsymbol{\beta}^*$ and γ_B^* , a basic grid-search method was employed.

A visual comparison of Figs. 4.1.2a and 4.1.2b shows that adding a reference signal to the transformation does not have a big impact on how the minimized H_∞ -norm varies with a_1 and a_2 . Indeed, the first three key observations made in Section 3.2 hold for this case as well.

Figures similar to Fig. 4.1.2a and 4.1.2b can be generated for $g_1 = g_2 = 1$. The plot of γ_B^* for the constant DC gain case looks similar to Fig. 3.2.1b, but now appears almost completely symmetrical. Similar to Corollary 2, $\gamma_B^* \rightarrow |g_1|/2$ when $a_1 \rightarrow 0$ for fixed a_2 , and also when $a_2 \rightarrow 0$ for fixed a_1 . The only difference is in the limit case. When $a_1 \neq 0$ and $a_2 = 0$, $\gamma_B^* = |g_1|/2$, but when $a_1 = 0$ and $a_2 = 0$, $\gamma_B^* = 0$. Qualitatively, the ratio plot of γ_B^*/γ_A^* looks very similar to Fig. 4.1.2b.

Key Observation 5: According to Fig. 4.1.2b, γ_A^* is always greater than γ_B^* . This shows that using the reference signal in the transformation reduces the least upper bound on the 2-norm of the transformation error; that is, γ_B^*/γ_A^* is smaller than one. The asymmetry in Fig. 4.1.2b shows that it is especially useful to do this when $a_2 < a_1$; that

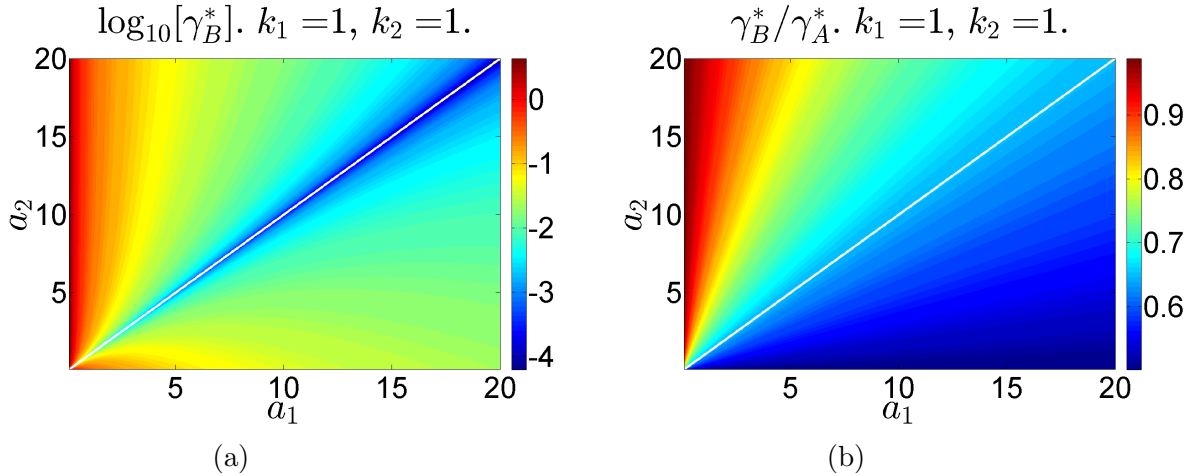


Figure 4.1.2: On the left, a contour plot of $\log_{10}[\gamma_B^*]$ vs. a_1 and a_2 is shown. The gains k_1 and k_2 are set to one to facilitate a fair comparison with γ_A^* . Here too, γ_B^* is zero when $a_1 = a_2$ and grows exponentially as the pole a_1 approaches zero. On the right, a contour plot illustrates the ratio γ_B^*/γ_A^* vs. a_1 and a_2 for $k_1 = 1$ and $k_2 = 1$. It can be seen that using the reference signal in the transformation always reduces the minimized H_∞ -norm of the system and the asymmetry reveals that the benefit of doing so is most evident when $a_2 < a_1$.

is, when the target system responds faster than the source system. The same observation holds for the OT analysis with constant DC gain.

4.2 Output Transfer Case – With Low-Pass Filter

The H_∞ analysis is useful for determining the worst-case transformation error for all the reference signals in set \mathcal{D} . However, this includes reference signals with high frequency components that are unrealistic in practice. For example, the blue signal in Fig. 4.2.1b has a 2-norm of about 0.8, but it is not one that a path-following robot would be expected to track. To address this, a low-pass filter (LPF) can be added to the transfer system in the OT case to filter out high-frequency components of $d(t)$ (see Fig. 4.2.1a). A first-order filter of the form

$$W(s) = \frac{a_W}{s + a_W} \quad (4.2.1)$$

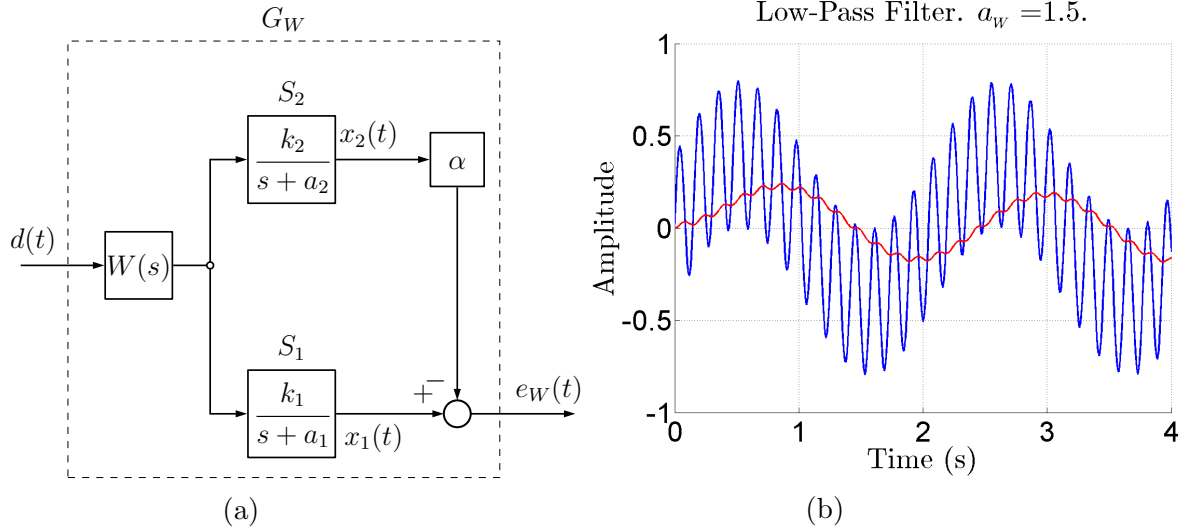


Figure 4.2.1: On the left is a block diagram of the OT case modified with a low-pass filter $W(s)$ added to the reference signal. On the right, the effect of a low-pass filter can be visualized; the high-frequency component of the blue signal is filtered out, leaving the red signal.

is chosen such that the DC gain of $W(s)$ is 1. The parameter a_W is assumed to always be positive and is chosen to be less than both a_1 and a_2 ,

$$a_W = \eta \min(a_1, a_2), \quad 0 < \eta < 1. \quad (4.2.2)$$

This is done so that the filter's cut-off frequency, that is, the frequency at which the magnitude of the signal begins to decrease from its nominal value, is lower than the cut-off frequency of the two systems S_1 and S_2 . For $a_W = 0.5$, the LPF produces the red signal in Fig. 4.2.1b.

While the error signal remains the same as in (3.1.3), $e_W = x_1(t) - \alpha x_2(t)$, the transfer function from $d(t)$ to $e_W(t)$ is

$$G_W(s) = \frac{a_W}{s + a_W} \left(\frac{k_1}{s + a_1} - \alpha \frac{k_2}{s + a_2} \right). \quad (4.2.3)$$

The transfer problem remains the same: minimizing $\|G_W\|_\infty$ with respect to α . In this problem, the H_∞ norm of G_W is found numerically over a search space of α . While the derivative of $|G_W(\omega, \alpha)|^2$ with respect to ω can be computed, finding its zeros analytically is a complicated task. The maximizing ω can be found by numerically finding

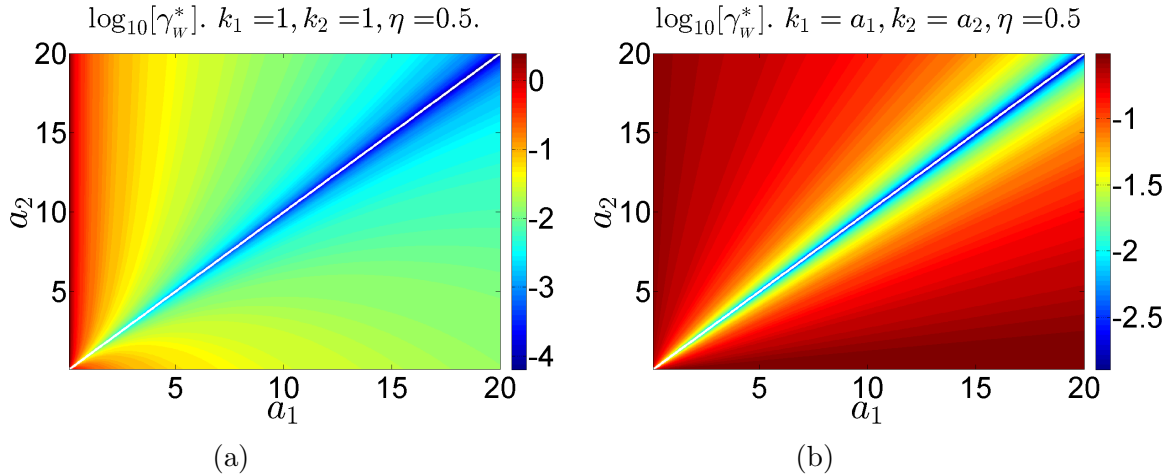


Figure 4.2.2: On the left is a contour plot of $\log_{10}[\gamma_W^*]$ vs. a_1 and a_2 for $k_1 = k_2 = 1$ and $\eta = .5$. On the right, the same plot for $g_1 = g_2 = 1$.

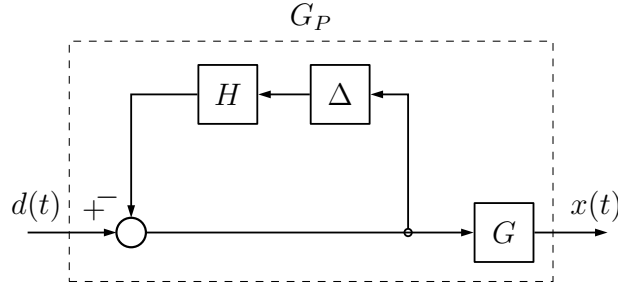
the zeros of this derivative, evaluating $|G_W(\omega, \alpha)|^2$ at these zeros, and finding the maximum value $\gamma_W(\alpha) := \max_{\omega} |G_W(\omega, \alpha)|$. Over a search space of α , the minimized H_{∞} norm, $\gamma_W^* := \gamma_W(\alpha^*)$, can be found.

If $a_1 = a_2$, $\alpha^* = k_1 k_2^{-1}$ and $\gamma_W^* = 0$. When $a_1 \neq a_2$, solutions can be found numerically. For $\eta = .5$, Figs. 4.2.2a-4.2.2b show how γ_W^* varies with the pole magnitudes, first when the gains are constant, and then when the DC gains are constant.

Key Observation 6: While it can be shown that $\gamma_W^* < \gamma_A^*$ as expected, we see that the variation of γ_W^* with a_1 and a_2 is similar to that of γ_A^* . However, we also see that γ_W^* is more symmetrical with respect to a_1 and a_2 than γ_A^* . For low-frequency reference signals, it matters less if the target or source system has a faster response.

4.3 Output Transfer Case – Pole Uncertainty

In this section, we analyze TL for two systems whose poles $-a_1$ and $-a_2$ are uncertain. This is done by using a technique from robust control to deal with the uncertainty in the system. We begin by adding uncertainty to one system.

Figure 4.3.1: Inverse multiplicative uncertainty added to a system G .

4.3.1 Adding Uncertainty to One System

If the pole of a first-order system of the form $G = k(s + a)^{-1}$ is uncertain, a new transfer function can be expressed as

$$G_P = \frac{k}{s + a(1 + r\delta)}, \quad (4.3.1)$$

where δ is an unknown scalar (the source of the uncertainty) constrained to the interval $[-1, 1]$, and r is a known scalar in the interval $[0, 1)$ used to express the degree of uncertainty of a , the nominal pole magnitude. Rearranging 4.3.1, G_P can be written as

$$G_P = \frac{G}{1 - H\Delta}, \quad (4.3.2)$$

where δ has been replaced by an unknown transfer function Δ that is subject to the constraint, $\|\Delta\|_\infty \leq 1$, and

$$H(s) := -\frac{ar}{s + a} \quad (4.3.3)$$

is a known weight. Note that the DC gain of $H(s)$ is r . The uncertainty of the transfer function expressed by the form in (4.3.2) is known as inverse multiplicative uncertainty [17] (see Fig. 4.3.1). Since Δ is unknown, $\|G_P\|_\infty$ cannot be evaluated. However, the known bound on $\|\Delta\|_\infty$ can be used to derive a bound on $\|G_P\|_\infty$.

Lemma 2. Let $G_P = G(1 - H\Delta)^{-1}$. If $\|\Delta\|_\infty \leq 1$ and $\|H\|_\infty < 1$, then

$$\|G_P\|_\infty \leq \frac{\|G\|_\infty}{1 - \|H\|_\infty}. \quad (4.3.4)$$

Proof. Since the H_∞ norm is sub-multiplicative,

$$\|G_P\|_\infty = \|G(1 - H\Delta)^{-1}\|_\infty \quad (4.3.5)$$

$$\leq \|G\|_\infty \|(1 - H\Delta)^{-1}\|_\infty. \quad (4.3.6)$$

The norm of $H\Delta$ has an upper bound of 1,

$$\|H\Delta\|_\infty \leq \|H\|_\infty \|\Delta\|_\infty, \quad (4.3.7)$$

$$\leq \|H\|_\infty, \quad (4.3.8)$$

$$< 1. \quad (4.3.9)$$

Using this bound and a result from geometric series,

$$\|(1 - H\Delta)^{-1}\|_\infty = \left\| \sum_{i=0}^{\infty} (H\Delta)^i \right\|_\infty, \quad (4.3.10)$$

$$\leq \sum_{i=0}^{\infty} \|(H\Delta)^i\|_\infty, \quad (4.3.11)$$

$$= \frac{1}{1 - \|H\Delta\|_\infty}, \quad (4.3.12)$$

$$\leq \frac{1}{1 - \|H\|_\infty}. \quad (4.3.13)$$

Putting everything together,

$$\|G_P\|_\infty \leq \frac{\|G\|_\infty}{1 - \|H\|_\infty}. \quad (4.3.14)$$

□

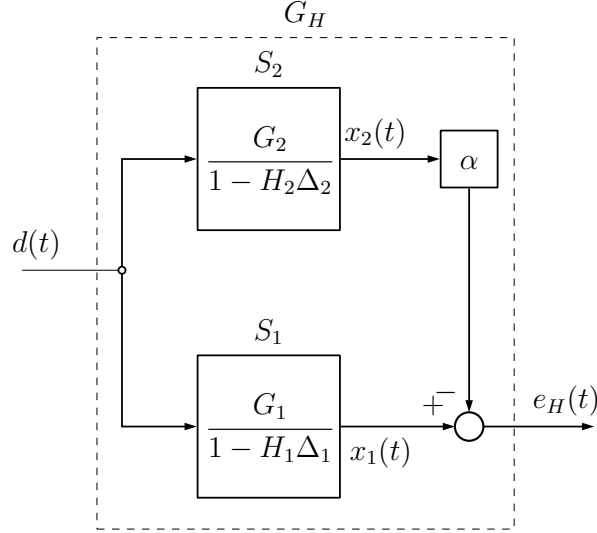


Figure 4.3.2: The OT case with inverse multiplicative uncertainty added to both systems.

4.3.2 Adding Uncertainty to the Transfer System

In this modified TL scenario, the α is computed to minimize an upper bound on $\|G_H\|_\infty$, where G_H is the transfer function from $d(t)$ to $e_H(t)$ in Fig. 4.3.2,

$$G_H = \frac{G_1}{1 - H_1\Delta_1} - \alpha \frac{G_2}{1 - H_2\Delta_2} \quad (4.3.15)$$

$$= \frac{G_1 - G_2\alpha - G_1H_2\Delta_2 + G_2H_1\Delta_1\alpha}{(1 - H_1\Delta_1)(1 - H_2\Delta_2)} \quad (4.3.16)$$

The same process to derive the upper bound in Section 4.3.1 can be used to derive an upper bound on $\|G_H\|_\infty$,

$$\|G_H\|_\infty \leq \rho(\alpha) := \frac{\|G_1 - G_2\alpha\|_\infty + \|G_1H_2\|_\infty + \|G_2H_1\alpha\|_\infty}{(1 - \|H_1\|_\infty)(1 - \|H_2\|_\infty)}. \quad (4.3.17)$$

The TL problem is then formulated as

$$\alpha^* := \arg \min_{\alpha} \rho(\alpha) \quad (4.3.18)$$

$$= \arg \min_{\alpha} (\|G_1 - G_2\alpha\|_\infty + \|G_2H_1\alpha\|_\infty). \quad (4.3.19)$$

Key Observation 7: In this uncertainty analysis, the optimal transformation α^* is independent of r_2 , the uncertainty of the source system.

The first term in the numerator of (4.3.17) is simply $\gamma_A^*(\alpha)$, $\|H_1\|_\infty$ and $\|H_2\|_\infty$ are r_1 and r_2 respectively, and

$$\|G_2 H_1 \alpha\|_\infty = |k_2 \alpha| \frac{r_1}{a_2}, \quad (4.3.20)$$

$$\|G_1 H_2\|_\infty = |k_1| \frac{r_2}{a_1}. \quad (4.3.21)$$

Let $\rho^* := \rho(\alpha^*)$. If $a_1 = a_2$, then

$$\alpha^* = \arg \min_{\alpha} \left(\frac{|k_1 - k_2 \alpha|}{a} + \frac{|k_2 \alpha| r_1}{a} \right) \quad (4.3.22)$$

The two points where the expression in (4.3.22) has local minima are $\alpha_{c1} = 0$ and $\alpha_{c2} = k_1 k_2^{-1}$. At these two points, the expression equals $|k_1| a^{-1}$ and $r_1 |k_1| a^{-1}$. Since $r_1 < 1$, the global minimum is at $\alpha^* = k_1 k_2^{-1}$ and

$$\rho^* = \frac{|k_1|}{a} \frac{r_1 + r_2}{(1 - r_1)(1 - r_2)}. \quad (4.3.23)$$

This result shows that if the systems have uncertain poles but their nominal poles are equal, then the best transformation is still the ratio of the gains of the two systems.

When $a_1 \neq a_2$, solutions can be found numerically. For $r_1 = r_2 = .2$, Fig. 4.3.3a shows how ρ^* varies with the pole magnitudes when $k_1 = k_2 = 1$. Fig. 4.3.3b shows the same plot when $g_1 = g_2 = 1$.

Key Observation 8: We see that when the DC gain is held constant, the upper bound on the H_∞ -norm is much greater than when the gains themselves are held constant.

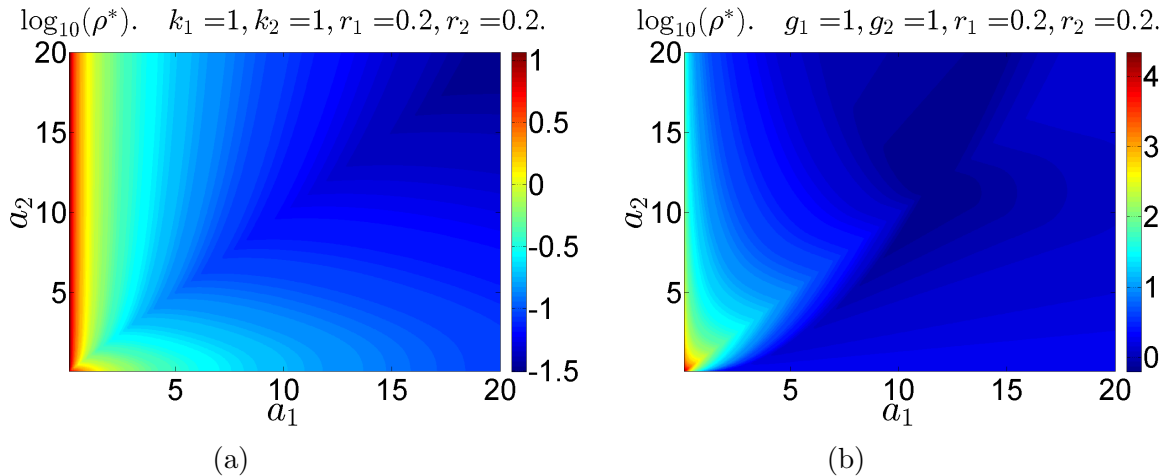


Figure 4.3.3: On the left is a contour plot of $\log_{10}[\rho^*]$ vs. a_1 and a_2 for $k_1 = k_2 = 1$ and $r_1 = r_2 = .2$. On the right, the same plot for $g_1 = g_2 = 1$.

4.4 Summary of Theoretical Results

We conclude this chapter with a summary of the results presented above. For two first-order, LTI, SISO systems, two ways to map to $x_1(t)$ for the purpose of TL were studied, Output Transfer and Input-Output transfer. The OT case was further studied by adding a low-pass filter to the reference signal and by considering pole uncertainty in the two systems. The following observations were made:

1. if the two systems are dynamically similar, that is, $a_1 \approx a_2$, the bound on the transformation error is small relative to if the systems are dynamically different;
2. for a fixed error bound, the two systems can be dynamically further apart if the poles are further from the imaginary axis;
3. the error bound is greater if the DC gain of the target system is greater;
4. the transformation error bound decreases if the reference signal is used, and more so if the target system has a faster response than the source system;
5. the addition of low-pass filter to the OT case does not markedly change how the error bound varies with a_1 and a_2 , but it does make the bound more symmetrical with respect to a_1 and a_2 ;

6. and, if pole uncertainty is introduced to the two systems, the optimal transformation α^* is independent of the uncertainty in the source system.

In general, we have seen how the stability properties of the two control systems influence the quality of the transformation. While these results may scale to higher order systems, the oscillatory behaviour of such systems will further contribute to how the transformation error varies with the system characteristics.

Chapter 5

Transfer Learning for 2D Wheeled Robots

We began the paper by making the argument that while TL for robotics has been shown to work before for specific examples, it has not been systematically studied. Therefore, our first novel result was the theoretical analysis of how the transfer error for first-order, LTI, SISO, systems relates to the system poles and gains, highlighting that the more dynamically similar the robots are, the better the transfer performance.

In this chapter, we perform a case study for two wheeled ground robots that can be modelled in the same way but vary parametrically. We use our theoretical results to study how well TL works for different pairs of source and target robots that vary in their control gains. For these different pairs of robots, data is generated in simulation and the transfer error 2-norm is compared to the error bound found from the H_∞ -norm minimization technique. Lastly, experimental data obtained from operating a Pioneer robot is used to learn a transformation and the error 2-norm computed. A comparison is made to the corresponding error 2-norm computed from simulation data.

5.1 Kinematic Model and Linearization about a Point Ahead

The 2D unicycle, depicted in Fig. 5.1.1a, has the pose $\mathbf{x} = [x, y, \theta]^T$ and its motion in an inertial frame can be modelled by the nonlinear kinematic equations,

$$\dot{x} = v \cos \theta, \quad (5.1.1)$$

$$\dot{y} = v \sin \theta, \quad (5.1.2)$$

$$\dot{\theta} = \omega, \quad (5.1.3)$$

where v and ω are the translational and rotational speeds. To analyze TL for the unicycle in the H_∞ framework, the model must first be linearized. To begin, we define the unicycle pose on the complex plane,

$$z = x + jy, \quad (5.1.4)$$

$$r = e^{j\theta}. \quad (5.1.5)$$

In this coordinate system, the unicycle model is

$$\dot{z} = rv, \quad (5.1.6)$$

$$\dot{r} = jr\omega. \quad (5.1.7)$$

We then linearize the unicycle about a point $p := z + \varepsilon r$ that is a distance $\varepsilon > 0$ ahead of the unicycle (see Fig. 5.1.1b). With a control input u , the linearized unicycle is then a kinematic integrator

$$\dot{p} = u. \quad (5.1.8)$$

By controlling the position of a point ahead of the robot, the rotation, and hence the non-linearity of the system is removed. To track a reference signal z_{ref} , a simple proportional

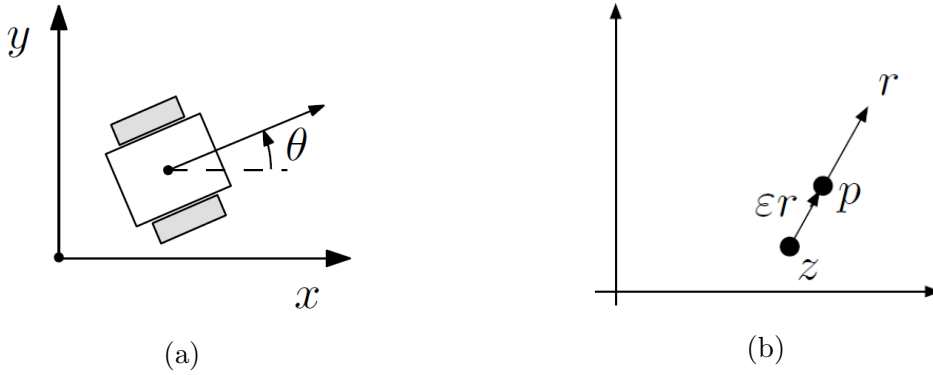


Figure 5.1.1: On the left is a depiction of a 2D wheeled robot. On the right is the position z of a unicycle on the complex plane with the point p ahead by distance ϵ .

controller with gain k can be devised,

$$u = k(z_{ref} - p). \quad (5.1.9)$$

The resulting closed-loop system is $G = k(s + k)^{-1}$ (see Fig. 5.1.2a). This is exactly the form of the system used in the TL analysis of the OT case with constant DC gain. In this analysis, the output of each system is the position of a point ahead of the unicycle in the complex plane: $p = p_x + jp_y$. However, it is more desirable to analyze 2D TL, where a time-invariant, 2×2 matrix \mathbf{A} is optimized to align the vector $[p_{x,2}, p_{y,2}]^T$ to $[p_{x,1}, p_{y,1}]^T$. To facilitate this, we modify the closed-loop system G to be multi-input, multi-output (MIMO) (see Fig. 5.1.2b). In the next section, we derive the H_∞ -norm of a 2D transfer system and minimize it with respect to the matrix \mathbf{A} .

But first, we derive nonlinear controllers for the translational and rotational velocities of the unicycle from the linearized model. Given that

$$\dot{p} = rv + jr\omega\epsilon, \quad (5.1.10)$$

the linear controller (5.1.9), and the error terms $e_x = x_{ref} - x$ and $e_y = y_{ref} - y$, the

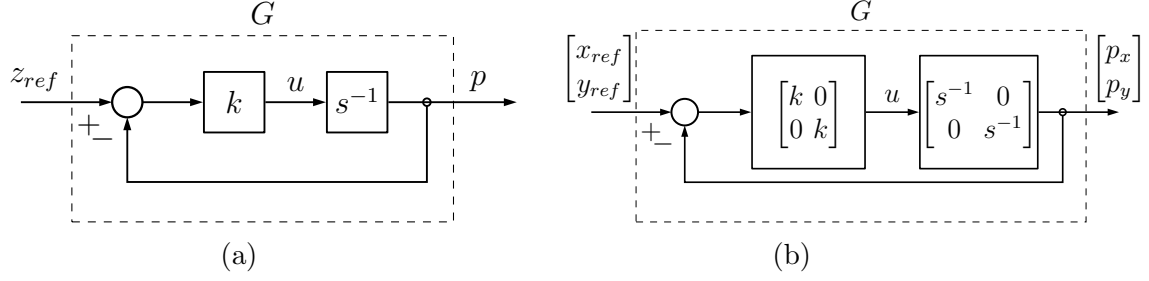


Figure 5.1.2: On the left, the closed-loop control block diagram for the linearized unicycle. On the right, a 2D decomposition of the linearized system.

kinematic integrator can be expanded,

$$rv + jr\omega\varepsilon = k(e_x + e_y - \varepsilon). \quad (5.1.11)$$

Two equations can be obtained by separating the real and imaginary components of (5.1.11), which can be solved for v and ω ,

$$v = k(e_x \cos \theta + e_y \sin \theta - \varepsilon), \quad (5.1.12)$$

$$\omega = \frac{k}{\varepsilon}(e_y \cos \theta - e_x \sin \theta). \quad (5.1.13)$$

These feedback controllers can control the nonlinear system (5.1.1):(5.1.3) in conjunction with constraints on v and ω to give a more realistic simulation of unicycle robots as well as to control the Pioneer robot in the indoor experiment.

5.2 Analysis of the Bound on the Transfer Error 2-Norm

The input of the 2D transfer system is $\mathbf{d} = [x_{ref}, y_{ref}]^T$, the output is

$$\mathbf{e}_A = \begin{bmatrix} p_{x,1} - (a_{1,1}p_{x,2} + a_{1,2}p_{y,2}) \\ p_{y,1} - (a_{2,1}p_{x,2} + a_{2,2}p_{y,2}) \end{bmatrix}, \quad (5.2.1)$$

and the transfer function is

$$\mathbf{G}_A(s) = \mathbf{G}_1 - \mathbf{A}\mathbf{G}_2. \quad (5.2.2)$$

For the 2D system, the H_∞ -norm of \mathbf{G}_A is the peak singular value of the matrix $\mathbf{G}_A(j\omega, \mathbf{A})$,

$$\|\mathbf{G}_A\|_\infty = \max_{\omega} \bar{\sigma}(\mathbf{G}_A(j\omega, \mathbf{A})). \quad (5.2.3)$$

The peak singular value is given by

$$\bar{\sigma} = \frac{\text{tr}(\mathbf{G}_A^H \mathbf{G}_A)}{2} + \sqrt{\left(\frac{\text{tr}(\mathbf{G}_A^H \mathbf{G}_A)}{2}\right)^2 - \det(\mathbf{G}_A^H \mathbf{G}_A)}, \quad (5.2.4)$$

where \mathbf{G}_A^H is the conjugate transpose of \mathbf{G}_A , $\text{tr}(\cdot)$ is the trace of the argument matrix, and $\det(\cdot)$ is the determinant of the argument matrix.

After numerically finding $\gamma_A := \min_{\mathbf{A}} \|\mathbf{G}_A\|_\infty$, we obtain the same result as in the OT case with constant DC gain. Indeed, if $\gamma_{\mathbf{A}}$ were to be found for various combinations of k_1 and k_2 , a figure identical to Fig. 3.2.1b would be obtained. In fact, we find that the optimal transformation matrix is simply

$$\mathbf{A}^* = \alpha^* \begin{bmatrix} 1 & 0 \\ 0 & 1 \end{bmatrix}, \quad (5.2.5)$$

where α^* is the optimal transformation found in the OT case with constant DC gain. That $a_{12}^* = a_{21}^* = 0$ is expected because of the diagonal nature of the transfer function matrices of the linearized unicycle model; that is, p_y is independent of x_{ref} and vice-versa. That $a_{11}^* = a_{22}^*$ is expected because the gains used in each of the two dimensions are the same.

5.3 Alignment-based Transfer Learning with Simulation Data

In this section, we demonstrate TL for datasets generated by tasking two linearized unicycle robots to follow a specific reference signal in simulation. Their models and controllers are given by (5.1.8) and (5.1.9) respectively.

For the simulation, the model and controller are discretized, resulting in the discrete-time equations

$$p[i + 1] = p[i] + \delta u[i] + n_{p,x} + j n_{p,y}, \quad n_{p,x}, n_{p,y} \sim \mathcal{N}(0, \sigma^2), \quad (5.3.1)$$

$$u[i] = k(z_{ref}[i] - p[i]), \quad (5.3.2)$$

where i and δ are the discrete-time index and time step, respectively. For a sampling rate of 200 Hz, δ is chosen to be 0.005. To the x and y dimensions, we separately add noise $n_{p,x}$ and $n_{p,y}$, which are Gaussian distributed with zero mean and variance σ^2 . The robots are tasked to follow an outward spiral trajectory $z_{ref} = x_{ref} + jy_{ref}$, where x_{ref} and y_{ref} are given by

$$x_{ref}(t) = \eta_3 \sin(\eta_1 t) e^{\eta_2 t}, \quad (5.3.3)$$

$$y_{ref}(t) = \eta_3 (\cos(\eta_1 t) e^{\eta_2 t} - 1). \quad (5.3.4)$$

The parameters $\eta_1 = .1$, $\eta_2 = .01$, and $\eta_3 = .03$ are chosen and the simulation is run for $4\pi/\eta_1 \approx 126$ seconds such that $\|z_{ref}\|_2 < 1$. Data is collected for $p_1[i]$, $p_2[i]$, and $z_{ref}[i]$, where $i \in \{1, 2, \dots, N\}$. Let \mathbf{P}_1 denote a $(N \times 1)$ matrix of samples of $p_1[i]$,

$$\mathbf{P}_1 = \begin{bmatrix} p_1[1] & \cdots & p_1[i] & \cdots & p_1[N] \end{bmatrix}^T. \quad (5.3.5)$$

Similarly, \mathbf{P}_2 is constructed from samples of $p_2[i]$. Let $\mathbf{M}_1 = [\text{Re}(\mathbf{P}_1^T), \text{Im}(\mathbf{P}_1^T)]^T$ and likewise for \mathbf{M}_2 . Then, by ordinary least-squares regression, an optimal $\bar{\alpha}$ is found such

that

$$\bar{\alpha} = \arg \min_{\alpha} \mathbf{E}_A^T \mathbf{E}_A, \quad (5.3.6)$$

where $\mathbf{E}_A := \mathbf{M}_1 - \alpha \mathbf{M}_2$. The solution is given by

$$\bar{\alpha} = \mathbf{M}_2^+ \mathbf{M}_1, \quad (5.3.7)$$

where $\mathbf{M}_2^+ = [\mathbf{M}_2^T \mathbf{M}_2]^{-1} \mathbf{M}_2^T$. The mapped trajectory in the complex plane is then

$$\hat{\mathbf{P}}_{1D} = \bar{\alpha} \mathbf{P}_2. \quad (5.3.8)$$

An estimate of the 2-norm of the error signal is then computed by trapezoidal integration,

$$\|e_A\|_2 = \sqrt{\frac{\delta}{2} \sum_{i=2}^N (|e_A[i]|^2 + |e_A[i-1]|^2)}, \quad (5.3.9)$$

$$e_A[i] = p_1[i] - \bar{\alpha} p_2[i]. \quad (5.3.10)$$

Here too, a 2×2 matrix $\bar{\mathbf{A}}$ can be found to optimally align the x and y position data of one unicycle to the other. Let $\mathbf{T} = [\text{Re}(\mathbf{P}_1), \text{Im}(\mathbf{P}_1)]$ and $\mathbf{S} = [\text{Re}(\mathbf{P}_2), \text{Im}(\mathbf{P}_2)]$. Then, a vector of the four optimal parameters in $\bar{\mathbf{A}}$, $\bar{\mathbf{a}} = [\bar{a}_{11}, \bar{a}_{12}, \bar{a}_{21}, \bar{a}_{22}]^T$, can be found by minimizing the sum squared error terms,

$$\bar{\mathbf{a}} = \arg \min_{\mathbf{a}} \mathbf{E}_A^T \mathbf{E}_A, \quad (5.3.11)$$

$$\mathbf{E}_A = \text{vec}(\mathbf{T}) - [\mathbf{I}_2 \otimes \mathbf{S}] \mathbf{a}, \quad (5.3.12)$$

where $\text{vec}(\cdot)$ transforms the argument matrix into a column vector, \mathbf{I}_2 is the 2×2 identity matrix, and \otimes is the Kronecker product operator; $[\mathbf{I}_2 \otimes \mathbf{S}]$ results in a $2N \times 4$ block diagonal matrix with \mathbf{S} on the diagonal and zeros elsewhere. Similar to (5.3.7), the

optimal transformation is given by

$$\bar{\mathbf{a}} = [\mathbf{I}_2 \otimes \mathbf{S}]^+ \text{vec}(\mathbf{T}). \quad (5.3.13)$$

The mapped trajectory in the complex plane is then constructed by using the first and second columns of the $N \times 2$ matrix $\mathbf{S}\bar{\mathbf{A}}$ as real and imaginary components,

$$\hat{\mathbf{P}}_{2D} = \mathbf{S}\bar{\mathbf{A}} \left(\begin{bmatrix} 1 \\ 0 \end{bmatrix} + j \begin{bmatrix} 1 \\ 0 \end{bmatrix} \right). \quad (5.3.14)$$

An estimate of the 2-norm of the 2D error signal is then computed by trapezoidal integration,

$$\|\mathbf{e}_A\|_2 = \sqrt{\frac{\delta}{2} \sum_{i=2}^N (\mathbf{e}_A[i] \mathbf{e}_A^T[i] + \mathbf{e}_A[i-1] \mathbf{e}_A^T[i-1])}, \quad (5.3.15)$$

$$\mathbf{e}_A[i] = \mathbf{T}[i] - \mathbf{S}[i]\bar{\mathbf{A}}. \quad (5.3.16)$$

Fig. 5.3.1a shows the trajectories of the target and source systems and the 1D and 2D alignments for $k_1 = 0.5$ and $k_2 = 1.25$, with noise variance $\sigma^2 = 1\text{E}-5$. Fig. 5.3.1b shows the 1D alignment (black) and the 2D alignment (green) errors, $|e_A[i]|$ and $\sqrt{\mathbf{e}_A[i] \mathbf{e}_A^T[i]}$ respectively, at each time step $i = 1, 2, \dots, N$, as well as the distance between the target and source systems' trajectories and the (blue), which acts as a control case.

Over the full time period, the estimates of the 2-norm of each error signal and of the control case are given in Table 5.3.1.

Table 5.3.1: The 2-norm of the 1D and 2D transformation errors and of the difference between the source and target trajectories.

$\ p_1 - p_2\ _2$	1.63
$\ e_A\ _2$	1.52
$\ \mathbf{e}_A\ _2$	0.69

Although the H_∞ analysis predicts that the performance of the 2D transformation will not improve over the 1D one, Fig. 5.3.1b and Table 5.3.1 show that the 2D transformation

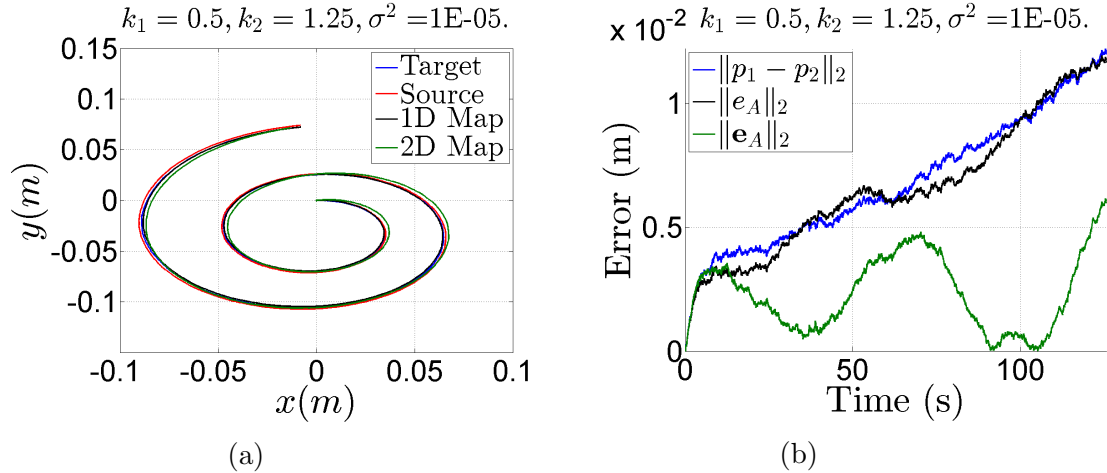


Figure 5.3.1: On the left, the two unicycle models move in the outward spiral. The TL objective is to align the red trajectory to the blue through \bar{a} for the 1D case (black line) and through $\bar{\mathbf{A}}$ for the 2D case (green line). On the right is a plot of the error distance at each time step of the simulation for the 1D case (black line), 2D case (green line), as well as the distance between both unicycle trajectories for comparison (blue line).

reduces the error. Indeed, we see that the 2×2 matrix learned from this data is

$$\bar{\mathbf{A}} = \begin{bmatrix} 0.9762 & 0.1146 \\ -0.0759 & 0.9773 \end{bmatrix}, \quad (5.3.17)$$

unlike \mathbf{A}^* in (5.2.5) from the H_∞ analysis, whose off-diagonal elements are 0.

We now see how the 2-norm of the transformation error varies for simulations that use different combinations of k_1 and k_2 in Fig 5.3.2a. Fig 5.3.2b illustrates the ratio of $\|e_A\|_2/\|e_A\|_2$ vs. k_1 and k_2 . A plot similar to Fig. 5.3.2a can be made by running the nonlinear model from (5.1.1):(5.1.3) with the nonlinear controller from (5.1.12):(5.1.13) in simulation. However, this plot is not included here due to the visual similarity with Fig. 5.3.2a.

From Fig. 5.3.2a, we see that $\|e_A\|_2$ varies in a way that is similar to γ_A^* without the constant DC gain in some regions, but varies similar to γ_A^* with the constant DC gain when $k_1 \gg k_2$. Specifically, we see that the asymmetry in Fig. 3.2.1b is preserved in Fig. 5.3.2a; that is, the transformation error is greater when $k_1 \gg k_2$, as compared to when $k_1 \ll k_2$.

We see from Fig. 5.3.2b that the error 2-norm is always lower when the 2D trans-

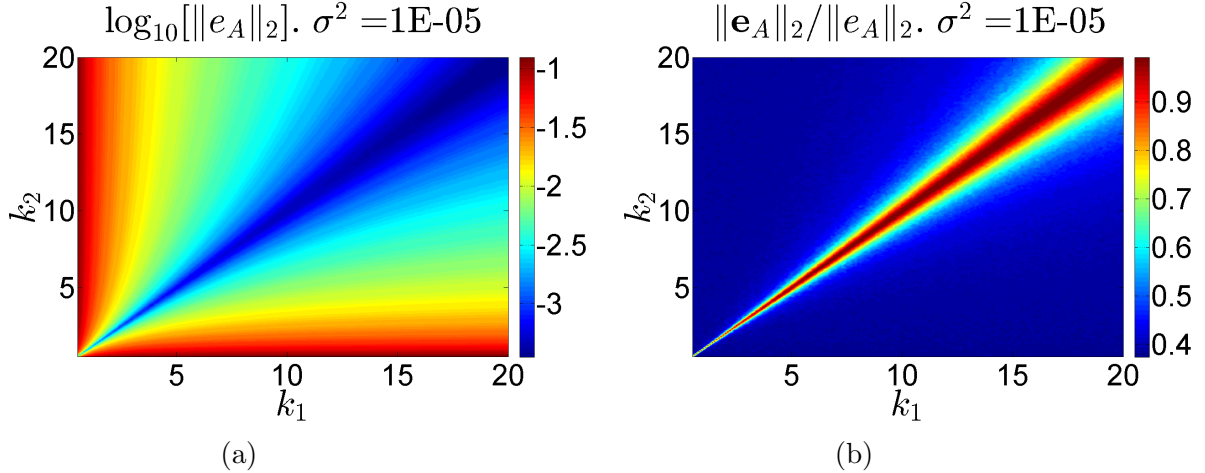


Figure 5.3.2: On the left is a contour plot of $\log_{10}[\|e_A\|_2]$ vs. k_1 and k_2 . On the right, a contour plot of $\|e_A\|_2 / \|e_A\|_2$ vs. k_1 and k_2 is shown. For both figures, $\sigma^2 = 1\text{E}-5$.

formation is used; that is, $\|e_A\|_2 < \|e_A\|_2$. However, when $k_1 \approx k_2$, there is no marked benefit of using the 2D transformation.

A more detailed comparison of $\|e_A\|_2$ and γ_W^* (OT case with constant DC gain and the low-pass filter) can be made by observing Figs. 5.3.3a and 5.3.3c. In each figure, line plots of the transformation error 2-norm or bound are shown for a fixed gain of one system and varying gain of the other system. Essentially, they are a cross-section of the contour plots Fig.5.3.2a and Fig. 4.2.2b. The blue plots are for fixed k_2 and the red plots are for fixed k_1 .

Furthermore, a cross section of $\|e_A\|_2$ computed from simulating the nonlinear system and controller is shown in Fig. 5.3.3b. For the simulation of the nonlinear model and controller, the distance of the point ahead was set to $\varepsilon = .1$. Constraints were imposed on the velocities; the allowable range for v and ω were $v \in [-v_{lim}, v_{lim}]$ and $\omega \in [-\omega_{lim}, \omega_{lim}]$, where $v_{lim} = 0.5 \text{ m s}^{-1}$ and $\omega_{lim} = 1.0 \text{ rad s}^{-1}$.

We see that the gap between the red and blue plots in Figs. 5.3.3a and 5.3.3b is much smaller than the corresponding gap in Fig. 5.3.3c. This indicates that $\|e_A\|_2$ is much more symmetrical than γ_W^* with respect to the system parameters (gains).

Key Observation 9: We have shown results from studying TL for two linearized unicycle models that are tasked to follow a specific reference signal in simulation. These results are dependent on the specific reference signal used and may vary for other reference

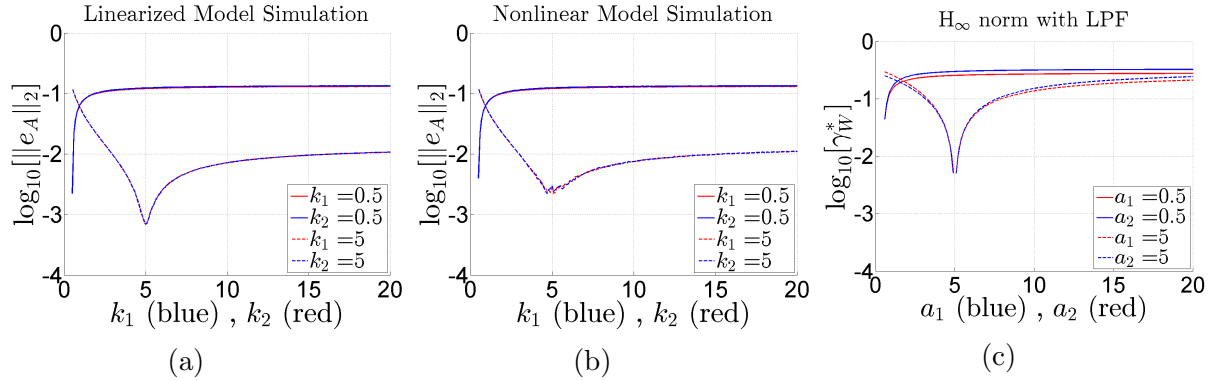


Figure 5.3.3: On the left are line plots of $\log_{10}[\|e_A\|_2]$ vs. k_1 for $k_2 = 0.5$ and $k_2 = 5$ (red) and the same vs. k_2 for $k_1 = 0.5$ and $k_1 = 5$ (blue), with noise $\sigma^2 = 1\text{E}-5$. In the centre are similar plots using data from simulating the nonlinear model and controller. On the right are similar line plots for $\log_{10}[\gamma_W^*]$ from the OT case with the constant DC gain and low-pass filter.

signals. However, the general trends of the error 2-norm are consistent with those of the error bound from the H_∞ analysis. In the next section, we show that this is also the case with experimental data.

5.4 Alignment-based Transfer Learning with Experimental Data

In this section, we obtain results similar to those in the previous section, but for data gathered in physical experiments with the Pioneer 3-AT, a small four-wheel drive, skid-steer robot (see Fig. 5.4.1a).

It is roughly 27 cm long (distance between front and rear wheel centres) and 50 cm wide. It can drive at a maximum speed of 0.7 m s^{-1} and turn at a maximum rate of 2.44 rad s^{-1} . However, we use the limits from the previous section, $v_{lim} = 0.5\text{ m s}^{-1}$ and $\omega_{lim} = 1.0\text{ rad s}^{-1}$. Considering these parameters, we choose $\eta_1 = 0.1$, $\eta_2 = .01$, $\eta_3 = .7$, and $\varepsilon = 0.1$ for an appropriate path to track.

For data acquisition, we use VICON, a motion capture system that uses active infrared cameras to provide the robot pose in an inertial frame at 200 Hz. The Pioneer is tasked to follow the path a few times, each time with a different controller gain. Although the robot's initial pose is different each time and not at the origin of the reference frame, the

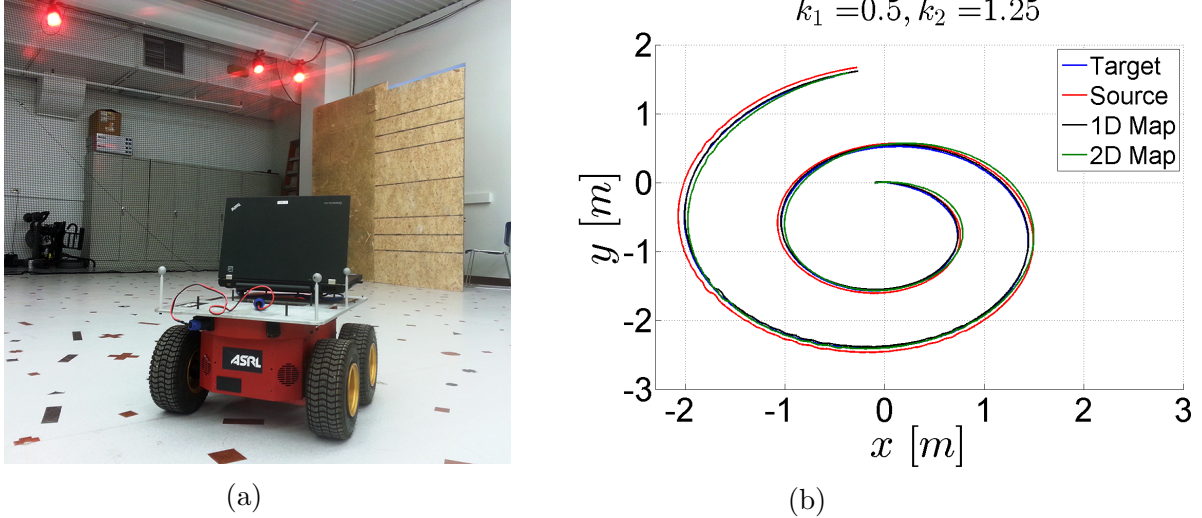


Figure 5.4.1: On the left is the Pioneer 3-AT robot in the VICON lab at UTIAS. On the right, the outward spiral trajectory traversed by the Pioneer robot using two different controller gains, $k_1 = 0.5$ (blue) and $k_1 = 1.25$ (red), and the alignment from red to blue is shown in black for the 1D transformation and green for the 2D transformation.

initial condition of the reference signal is subtracted from the collected data; that is,

$$x[i] = x[i] - x_{ref}[1], \quad (5.4.1)$$

for all time steps $i \in \{1, 2, \dots, N\}$, and likewise for $y[i]$. The initial condition for the robot's orientation is $\theta[1] = 0$. The number of data points collected, N , is different each time. To obtain time-synchronized data that can be used in the TL algorithm, the pose from one dataset is interpolated at the time steps of the other dataset and vice-versa. Duplicate values that occur at time steps that are common between both datasets are removed.

Figure 5.4.1b shows two trajectories of the Pioneer with different controller gains, $k_1 = 0.5$ (blue) and $k_2 = 1.25$ (red). The black and green lines are the alignment curves from the 1D and 2D least-squares TL algorithm, where an optimal scalar $\bar{\alpha}$ and matrix $\bar{\mathbf{A}}$ are found respectively. The corresponding error plot is shown in Fig. 5.4.2.

Estimates for $\|e_A\|_2$ and $\|\mathbf{e}_A\|_2$ are 1.52 and 0.69. If the source and target gains are swapped, that is, if $k_1 = 1.25$ and $k_2 = 0.5$, $\|e_A\|_2$ and $\|\mathbf{e}_A\|_2$ increase to 1.56 and 0.72, as expected from our theoretical analysis.

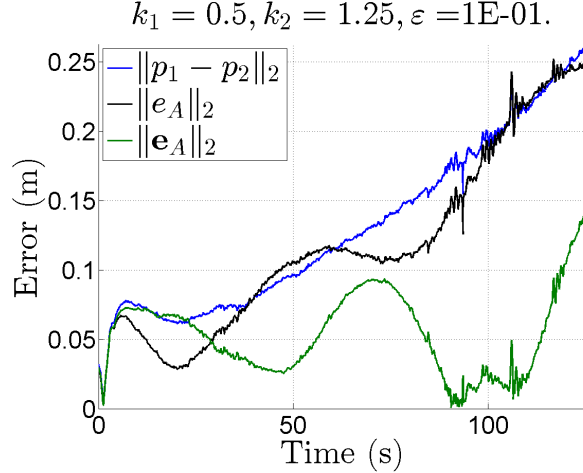


Figure 5.4.2: A plot of the error distance at each time step of the experiment for the 1D case (black line), 2D case (green line), as well as the distance between both Pioneer trajectories for comparison (blue line).

For other combinations of k_1 and k_2 , $\|e_A\|_2$ is given in Table 5.4.1. In this table, the difference between k_1 and k_2 is held constant at 0.25. We observe that

1. as k_1 and k_2 increase in magnitude, $\|e_A\|_2$ decreases (relates to **Key Observation 2** from Section 3.2);
2. if k_1 and k_2 are small, the difference between $\|e_A\|_2$ for the cases $k_1 > k_2$ and $k_1 < k_2$ is larger than if k_1 and k_2 are larger (relates to **Key Observation 3** from Section 3.2); for example, the difference between $\|e_A\|_2$ for the cases $\{k_1 = 0.5, k_2 = 0.75\}$ and $\{k_1 = 0.75, k_2 = 0.5\}$ is 0.013, but for the cases $\{k_1 = 1.0, k_2 = 1.25\}$ and $\{k_1 = 1.25, k_2 = 1.0\}$, the difference is 0.001;
3. if $k_1 > k_2$, $\|e_A\|_2$ is greater than if $k_1 < k_2$ (relates to **Key Observation 4** from Section 3.2).

These observations are consistent with the results from the simulations and H_∞ analysis.

Table 5.4.1: A table of $\|e_A\|_2$ for different gain combinations used in the Pioneer experiment.

k_1	k_2	$\ e_A\ _2$
0.5	0.75	0.768
0.75	1.0	0.497
1.0	1.25	0.276
0.75	0.5	0.781
1.0	0.75	0.501
1.25	1.0	0.277

5.5 Summary

In this chapter, we studied TL for 2D wheeled robots. First, the H_∞ analysis was done for two kinematic unicycle models, each linearized about a point ahead of the unicycle. Then, the unicycle models were tasked to follow an outward spiral trajectory in simulation for various combinations of target and source system gains. For each combination, an estimate of the transfer error 2-norm was computed. For all combinations, the error 2-norm was compared to the error bound from the H_∞ analysis. This was repeated for the error 2-norm computed from simulating the nonlinear unicycle system with a nonlinear controller and velocity constraints. It was shown that the 2-norm from the simulations varied with the system parameters in a similar way to the error bound. Lastly, experimental data was obtained from a Pioneer robot following the spiral trajectory indoors for a few different controller gains. By computing and comparing the transfer error 2-norm for a few combinations of these gains, it was shown that the results were consistent with those from the simulations and H_∞ analysis.

Chapter 6

Conclusions and Outlook

A robot's path-tracking performance has been shown to improve by using data-driven learning techniques. Can the source of this data be another robot? How feasible is Transfer Learning for robotics?

To begin to quantitatively answer these questions, a simplified scenario that involved two first-order, LTI, SISO systems was studied. In this scenario, an LTI, scalar transformation is used to map the output from one system to the output from another - the Output Transfer (OT) case. By framing this as an H_∞ -norm minimization problem, an upper bound on the 2-norm of the transformation error is derived and minimized with respect to the transformation scalar. This minimized error bound is a measure of the quality of TL.

The bound is shown to grow with the DC gain of S_1 , the target system. It is reduced when the systems are dynamically similar; that is, when the poles of the systems are located close to each other. For systems with larger pole magnitudes, the poles can be located further apart from each other for the same error bound.

Extensions to the OT case were then studied. In the first, the reference signal is included in the transformation, and the error bound was reduced further. In the second, a low-pass filter was added to the reference signal in order to filter out the high frequency components of the signal and perform a more realistic analysis of the variation of the error bound. While keeping the DC gain of the target system, we see that the error bound varies with the system poles more symmetrically than without the low-pass filter.

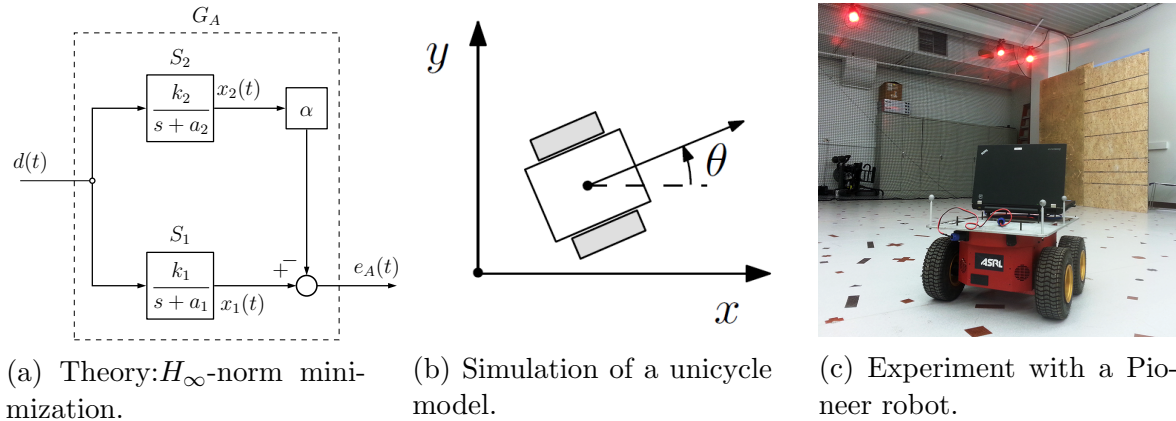


Figure 6.0.1: A summary of the tools used to study TL in this project.

In the third, pole uncertainty was added to each of the two systems and the least upper bound on the H_∞ -norm of the transfer system derived. It was shown that in the OT case, this new bound was greater when the DC gain is held constant.

Overall, the theoretical results provide initial insight to the problem of learning a map between data from two control systems. These results can be further extended for higher order systems. It is expected that the location of the poles closest to the imaginary axis will have more impact on the transfer quality. However, the transfer quality will also be affected by the oscillatory behaviour of such systems.

In addition to these results, TL was studied for 2D wheeled robots. The nonlinear, kinematics model of a unicycle was linearized about a point ahead and its control loop closed by a proportional controller. The resulting system was shown to be a special case of the general first-order, LTI, SISO system studied in the OT case. The system was then modified to be MIMO, where the transformation applied on the 2D output, x and y , is a 2×2 matrix. It was shown that this had no effect on the error bound since the control of the x and y dimensions are independent of each other.

The two linearized unicycle models, each with a different controller gain, were then tasked to follow a spiral trajectory in simulation. An estimate of the 2-norm of the transfer error was computed for several combinations of the two system gains. It was shown that the variation of this 2-norm was consistent with the variation of the error bound from the H_∞ analysis of the OT case with the constant DC gain and low-pass

filter, though the error 2-norm varied more symmetrically with the system parameters than the error bound. This analysis was repeated for simulations with the nonlinear unicycle models and velocity constraints. Lastly, we showed similar results using data obtained from indoor experiments with a Pioneer robot.

Appendix A

Proof for Lemma 1

Proof. Note that all four λ parameters in (3.2.4)-(3.2.7) are non-negative, and that λ_1 and λ_2 are functions of α . To reduce clutter, $\lambda_1(\alpha)$ and $\lambda_2(\alpha)$ are denoted by λ_1 and λ_2 in the remainder of the paper. If $a_1, a_2 > 0$, then for all $\alpha \in \mathbb{R}$,

$$\lim_{\omega \rightarrow \pm\infty} |G_A(j\omega, \alpha)|^2 = 0. \quad (\text{A.1})$$

Let the frequency that maximizes the squared magnitude for a given value of α be

$$\omega^*(\alpha) = \arg \max_{\omega} |G_A(j\omega, \alpha)|^2. \quad (\text{A.2})$$

The maximum of $|G_A(j\omega, \alpha)|^2$ can be obtained by finding the roots of the derivative of $|G_A(j\omega, \alpha)|^2$ with respect to ω ,

$$\frac{\partial |G_A(j\omega, \alpha)|^2}{\partial \omega} = 0 \quad (\text{A.3})$$

$$\Leftrightarrow \frac{-2\omega (\lambda_1\omega^4 + 2\lambda_2\omega^2 + \lambda_2\lambda_4 - \lambda_1\lambda_5)}{(\omega^4 + \lambda_4\omega^2 + \lambda_5)^2} = 0 \quad (\text{A.4})$$

$$\Leftrightarrow \omega (\lambda_1\omega^4 + 2\lambda_2\omega^2 + \lambda_2\lambda_4 - \lambda_1\lambda_5) = 0 \quad (\text{A.5})$$

$$\Leftrightarrow \omega \left(\frac{1}{4}\omega^4 + p(\alpha)\omega^2 + q(\alpha) \right) = 0, \quad (\text{A.6})$$

where

$$p(\alpha) = \frac{\lambda_2}{2\lambda_1}, \quad (\text{A.7})$$

$$q(\alpha) = \frac{\lambda_2\lambda_4 - \lambda_1\lambda_5}{4\lambda_1}. \quad (\text{A.8})$$

In (A.5), the equation is divided by $4\lambda_1$ to obtain a standard form of the quartic term in (A.6), whose roots are known functions of $p(\alpha)$ and $q(\alpha)$ (see Appendix C). Note that $p(\alpha)$ is always non-negative, whereas $q(\alpha)$ can be negative. Case C2 in Appendix C is not possible since if $p(\alpha) = 0$, then $q(\alpha) = -\lambda_5/4 < 0$, contradicting case C2.

To find $\max_{\omega} |G_A(j\omega, \alpha)|^2$, the real roots of the polynomial in (A.6) need to be found. Therefore, there are two cases of interest:

Case 1: This case corresponds to cases C1 and C3 from Appendix C, and considers $q(\alpha) \geq 0$. In this case, the only real root of (A.6) is 0. After verifying that $\omega = 0$ is a local maximum of $\|G_A(j\omega, \alpha)\|^2$ with the second derivative, we obtain $\omega^* = 0$ for all α due to (A.1). Therefore,

$$\|G_A\|_{\infty}^2 = |G_A(0j, \alpha)|^2 \quad (\text{A.9})$$

$$= \frac{\lambda_2}{\lambda_5} \quad (\text{A.10})$$

$$= \frac{(k_1a_2 - k_2a_1\alpha)^2}{a_1^2a_2^2} := \psi(\alpha). \quad (\text{A.11})$$

As a result, $\|G_A\|_{\infty}^2$ is a quadratic function of α .

Case 2: This case corresponds to case C4 from Appendix C, and considers $q(\alpha) < 0$. In this case, there are three real roots. In addition to the real root $\omega_1 = 0$, the quartic term has two real roots $\pm\omega_2$. Since there are three real roots with non-zero second derivative and because of (A.1), the vertices at $\pm\omega_2$ must be maxima and the vertex at $\omega_1 = 0$ must

be a minimum. Therefore,

$$(\omega^*(\alpha))^2 = \omega_2^2 \quad (\text{A.12})$$

$$= 2\sqrt{p^2(\alpha) - q(\alpha)} - 2p(\alpha) \quad (\text{A.13})$$

$$= \frac{\sqrt{\lambda_2^2 - \lambda_1\lambda_2\lambda_4 + \lambda_1^2\lambda_5} - \lambda_2}{\lambda_1}. \quad (\text{A.14})$$

Evaluating (3.2.3) at $\omega^2 = \omega_2^2$ results in

$$\|G_A\|_\infty^2 = |G_A(\pm\omega_2 j, \alpha)|^2 \quad (\text{A.15})$$

$$= \frac{\lambda_1^2}{g(\alpha) + 2\sqrt{f(\alpha)}} := \phi(\alpha), \quad (\text{A.16})$$

where

$$f(\alpha) := \lambda_5\lambda_1^2 - \lambda_4\lambda_1\lambda_2 + \lambda_2^2, \quad (\text{A.17})$$

$$g(\alpha) := \lambda_4\lambda_1 - 2\lambda_2. \quad (\text{A.18})$$

In this case, $\|G_A\|_\infty^2$ is a nonlinear function of α .

The last step in proving Lemma 1 is to re-work the conditions in Case 1 and Case 2, which are expressed in terms of $q(\alpha)$ and not α .

We first consider the special case where $a_2 = a_1 = a$. Then $q(\alpha) = a^4/4$. In this case, $q(\alpha) > 0$ for all α and according to (A.11),

$$\|G_A\|_\infty^2 = \frac{(k_1 - \alpha k_2)^2}{a^2}. \quad (\text{A.19})$$

Since (A.19) is quadratic in α , a unique minimizing α exists:

$$\alpha = \frac{k_1}{k_2}, \quad (\text{A.20})$$

which is the ratio of the system gains.

When $a_2 \neq a_1$, $q(\alpha)$ can be negative. To obtain a solution, we find the roots of $q(\alpha)$

by solving

$$0 = q(\alpha) \tag{A.21}$$

$$\Leftrightarrow 0 = \lambda_2 \lambda_4 - \lambda_1 \lambda_5 \tag{A.22}$$

$$\Leftrightarrow 0 = (a_1^4 k_2^2) \alpha^2 - (2a_1 a_2 k_1 k_2 (a_1^2 - a_1 a_2 + a_2^2)) \alpha + (a_2^4 k_1^2). \tag{A.23}$$

We obtain two real roots:

$$\alpha_1 = \frac{k_1 a_2}{k_2 a_1^3} (a_1^2 + a_2^2 - a_1 a_2 + \sqrt{(a_1 - a_2)^2 (a_1^2 + a_2^2)}), \tag{A.24}$$

$$\alpha_2 = \frac{k_1 a_2}{k_2 a_1^3} (a_1^2 + a_2^2 - a_1 a_2 - \sqrt{(a_1 - a_2)^2 (a_1^2 + a_2^2)}). \tag{A.25}$$

It is clear that $\alpha_2 < \alpha_1$ for all $a_1, a_2 > 0$, k_1 , and $k_2 \neq 0$. When $\alpha \leq \alpha_2$ or $\alpha \geq \alpha_1$, $q(\alpha) \geq 0$ and $\|G_A\|_\infty^2 = \psi(\alpha)$. When $\alpha_2 < \alpha < \alpha_1$, $q(\alpha) < 0$ and $\|G_A\|_\infty^2 = \phi(\alpha)$. To summarize, $\|G_A\|_\infty^2$ and $\omega^*(\alpha)$ are piecewise functions of α and are given by

$$\gamma_A^2(\alpha) := \|G_A\|_\infty^2 = \begin{cases} \phi(\alpha) & \text{if } \alpha_2 < \alpha < \alpha_1 \\ \psi(\alpha) & \text{otherwise} \end{cases}, \tag{A.26}$$

$$\omega^*(\alpha) = \begin{cases} \pm \omega_2 & \text{if } \alpha_2 < \alpha < \alpha_1 \\ 0 & \text{otherwise} \end{cases}, \tag{A.27}$$

with

$$\omega_2 := \sqrt{2\sqrt{p^2(\alpha) - q(\alpha)} - 2p(\alpha)}.$$

To prove continuity of $\gamma_A(\alpha)$, it must be shown that

- (i) $\psi(\alpha)$ is continuous in the intervals $(-\infty, \alpha_2]$ and $[\alpha_1, \infty)$,
- (ii) $\phi(\alpha)$ is continuous in the open interval (α_2, α_1) ,
- (iii) and that $\phi(\alpha_1) = \psi(\alpha_1)$ and $\phi(\alpha_2) = \psi(\alpha_2)$ for all $a_1, a_2 > 0$, k_1 , and $k_2 \neq 0$.

The first condition is true because $\psi(\alpha)$ is a polynomial and is thus continuous over its domain.

Secondly, the function $\phi(\alpha)$ is continuous under the following two conditions:

1. We first make sure that the square-root term in (A.16) is well-defined:

$$0 \leq f(\alpha) \tag{A.28}$$

$$= k_1 k_2 (a_1 - a_2)^2 \left[(2a_1 k_2^2 (a_1 + a_2)) \alpha^2 + (-k_1 k_2 (a_1^2 + 6a_1 a_2 + a_2^2)) \alpha + 2a_2 k_1^2 (a_1 + a_2) \right] \alpha. \tag{A.29}$$

The inequality is true when $\alpha \geq \alpha_{f,1}$ and $0 \leq \alpha \leq \alpha_{f,2}$, where

$$\alpha_{f,1} = \frac{k_1 (a_1 + a_2)}{k_2 \frac{2a_1}{2a_1}}, \tag{A.30}$$

$$\alpha_{f,2} = \frac{k_1 \frac{2a_2}{2a_2}}{k_2 (a_1 + a_2)}. \tag{A.31}$$

It can be shown that $\alpha_{f,1} > \alpha_{f,2}$ for all $a_1, a_2 > 0$, k_1 , and $k_2 \neq 0$. To show that the inequality in (A.29) is true over the interval (α_2, α_1) , it can be shown that either $\alpha_{f,2} > \alpha_1$ or that $\alpha_{f,1} < \alpha_2$; that is, $\alpha_{f,2}, \alpha_{f,1} \notin (\alpha_2, \alpha_1)$.

2. The second condition is that

$$g(\alpha) + 2\sqrt{f(\alpha)} \neq 0. \tag{A.32}$$

To satisfy (A.32), $\alpha \neq \alpha_0$ with $\alpha_0 := k_1 k_2^{-1}$ because

$$0 = f(\alpha) - \frac{g^2(\alpha)}{4} \tag{A.33}$$

$$= -\frac{(a_1^2 - a_2^2)^2 (k_1 - \alpha k_2)^4}{4}. \tag{A.34}$$

It can be shown that either $\alpha_0 < \alpha_2$, or $\alpha_0 > \alpha_1$, for all $a_1, a_2 > 0$, k_1 , and $k_2 \neq 0$.

Therefore, $\phi(\alpha)$ is continuous in the open interval (α_2, α_1) .

The third condition can be shown to be true by evaluating $\phi(\alpha)$ and $\psi(\alpha)$ at α_1 and α_2 . We used analytic simplification techniques in MATLAB to determine that for

all $a_1, a_2 > 0$, k_1 , and $k_2 \neq 0$, $\phi(\alpha_1) = \psi(\alpha_1)$ and $\phi(\alpha_2) = \psi(\alpha_2)$.

□

Appendix B

Proof for Theorem 1

Proof. To find the minimum of $\gamma_A^2(\alpha)$, one possibility is to find the minimum of $\phi(\alpha)$ for all $\alpha \in (\alpha_2, \alpha_1)$ and the minimum of $\psi(\alpha)$ for all $\alpha \notin (\alpha_2, \alpha_1)$, and then compare the two. However, it can be shown that $\alpha_2 < \alpha^* < \alpha_1$ for all $a_1, a_2 > 0$, k_1 , and $k_2 \neq 0$, thereby limiting the search for the minimum to $\phi(\alpha)$. To prove that $\alpha_2 < \alpha^* < \alpha_1$, one can use Bolzano's Theorem [14], which considers the derivative of $\phi(\alpha)$ with respect to α denoted by $\phi'(\alpha)$ and states: if $\phi'(\alpha)|_{\alpha=\alpha_2} < 0$ and $\phi'(\alpha)|_{\alpha=\alpha_1} > 0$, then $\phi'(\alpha)$ has a minimum in the interval (α_2, α_1) . MATLAB can be used to check the aforementioned conditions on $\phi'(\alpha)$ at the points α_1 and α_2 . However, it is easier to validate that $\phi'(\alpha) = \psi'(\alpha)$ at α_1 and α_2 , and use the fact that $\psi(\alpha)$ satisfies the above conditions. The function $\psi(\alpha)$ is a convex parabola with a single minimum at

$$\alpha_\psi = \frac{k_1 a_2}{k_2 a_1}. \quad (\text{B.1})$$

It is sufficient to show that $\alpha_2 < \alpha_\psi < \alpha_1$ for all $a_1, a_2 > 0$, k_1 , and $k_2 \neq 0$.

It now remains to find α^* by solving $\phi'(\alpha) = 0$. The derivative $\phi'(\alpha)$ is

$$\phi'(\alpha) = -\frac{2k_2 h^3(\alpha)}{(2(\sqrt{f(\alpha)} - \lambda_2) + \lambda_4 \lambda_1)^2} \left(4\sqrt{f(\alpha)} + 2g(\alpha) + h(\alpha)z_2(\alpha) \right), \quad (\text{B.2})$$

where

$$z_2(\alpha) = m(\alpha) + \frac{n(\alpha)}{\sqrt{f(\alpha)}}, \quad (\text{B.3})$$

$$h(\alpha) = \sqrt{\lambda_1}, \quad (\text{B.4})$$

$$m(\alpha) = (a_2 - a_1) (k_2 (a_1 + a_2) \alpha - k_1 (a_2 - a_1)), \quad (\text{B.5})$$

$$n(\alpha) = k_1 (a_2 - a_1)^2 ((a_1 + a_2) (3a_1 k_2^2 \alpha^2 + a_2 k_1^2) - k_1 k_2 (a_1^2 + 6a_1 a_2 + a_2^2) \alpha). \quad (\text{B.6})$$

Besides the three roots at $a_0 = k_1 k_2^{-1}$ found from the term $h^3(\alpha)$ in (B.2), the other roots of $\phi'(\alpha)$ are found by solving

$$0 = 4\sqrt{f(\alpha)} + 2g(\alpha) + h(\alpha)z_2(\alpha). \quad (\text{B.7})$$

As it was previously shown that $f(\alpha) \geq 0$ in the interval (α_2, α_1) , further modifications of (B.7) result in a new equation to solve for α :

$$f(\alpha) = \left(\frac{4f(\alpha) + n(\alpha)h(\alpha)}{2g(\alpha) + m(\alpha)h(\alpha)} \right)^2 \quad (\text{B.8})$$

$$\Leftrightarrow 0 = f(\alpha) (2g(\alpha) + m(\alpha)h(\alpha))^2 - (4f(\alpha) + n(\alpha)h(\alpha))^2 \quad (\text{B.9})$$

$$\Leftrightarrow 0 = (k_1 - k_2 \alpha)^5 (2k_2^2 a_1 (a_1 + a_2) \alpha^2 - a_2 k_1 k_2 (4a_1 + a_2) \alpha + a_2^2 k_1^2). \quad (\text{B.10})$$

In addition to the several roots at α_0 , the quadratic expression in (B.10) yields two real roots:

$$\alpha_{\phi,1} = \frac{k_1}{k_2} \frac{2a_2}{\left(4a_1 + a_2 - \sqrt{8a_1^2 + a_2^2}\right)}, \quad (\text{B.11})$$

$$\alpha_{\phi,2} = \frac{k_1}{k_2} \frac{2a_2}{\left(4a_1 + a_2 + \sqrt{8a_1^2 + a_2^2}\right)}. \quad (\text{B.12})$$

One can show that $\alpha_2 < \alpha_{\phi,1} < \alpha_1$ and $\phi'(\alpha)|_{\alpha=\alpha_{\phi,1}} = 0$ for all $a_1, a_2 > 0$, k_1 , and $k_2 \neq 0$. The same is not true for $\alpha_{\phi,2}$, which represents a degenerate case obtained by squaring (B.7). Therefore, $\alpha^* = \alpha_{\phi,1}$. \square

Appendix C

Roots of the Biquadratic Equation

Consider the general biquadratic equation,

$$\frac{1}{4}x^4 + px^2 + q = 0. \quad (\text{C.1})$$

The discriminant of this equation is given by

$$D = q(p^2 - q). \quad (\text{C.2})$$

The four roots of the biquadratic equation are given in terms of p and q for four cases:

Case C1: For $q > p^2$, there are four complex roots,

$$x_{1,2,3,4} = \pm\sqrt{\sqrt{q} - p} \pm j\sqrt{\sqrt{q} + p}. \quad (\text{C.3})$$

Case C2: For $p \leq 0 \leq q \leq p^2$, there are four real roots,

$$x_{1,2,3,4} = \pm\sqrt{\sqrt{q} - p} \pm \sqrt{-\sqrt{q} - p}. \quad (\text{C.4})$$

Case C3: For $p > 0$ and $0 \leq q \leq p^2$, there are four roots with zero real part,

$$x_{1,2,3,4} = j(\pm\sqrt{p + \sqrt{q}} \pm \sqrt{p - \sqrt{q}}). \quad (\text{C.5})$$

Case C4: For, $q < 0$, there are two real roots and two roots with zero real part,

$$x_{1,2} = \pm \sqrt{2\sqrt{p^2 - q} - 2p}, \quad (\text{C.6})$$

$$x_{3,4} = \pm j \sqrt{2\sqrt{p^2 - q} + 2p}. \quad (\text{C.7})$$

Bibliography

- [1] Muhammad Arif, Tadashi Ishihara, and Hikaru Inooka. Incorporation of experience in iterative learning controllers using locally weighted learning. *Automatica*, 37(6):881–888, 2001.
- [2] Felix Berkenkamp and Angela P. Schoellig. Safe and robust learning control with Gaussian processes. In *Proc. of the European Control Conference (ECC)*, pages 2501–2506, 2015.
- [3] Botond Bocsi, Lehel Csató, and Jan Peters. Alignment-based transfer learning for robot models. In *Proc. of the 2013 International Joint Conference on Neural Networks (IJCNN)*, pages 1–7, 2013.
- [4] Georgios Boutsioukis, Ioannis Partalas, and Ioannis Vlahavas. Transfer learning in multi-agent reinforcement learning domains. In *Recent Advances in Reinforcement Learning*, pages 249–260. Springer, 2012.
- [5] John Comstock Doyle, Bruce A Francis, and Allen Tannenbaum. *Feedback control theory*, volume 1. Macmillan Publishing Company New York, 1992.
- [6] Jihun Ham, Daniel Lee, and Lawrence Saul. Semisupervised alignment of manifolds. In *Proc. of the Annual Conference on Uncertainty in Artificial Intelligence*, volume 10, pages 120–127, 2005.
- [7] Michael Hamer, Markus Waibel, and Raffaello D’Andrea. Knowledge transfer for high-performance quadcopter maneuvers. In *Proc. of the IEEE/RSJ International Conference on Intelligent Robots and Systems (IROS)*, pages 1714–1719, 2013.

- [8] Pieter Janssens, Goele Pipeleers, and Jan Swevers. Initialization of ILC based on a previously learned trajectory. In *Proc. of the American Control Conference (ACC)*, pages 610–614, 2012.
- [9] Balaji Lakshmanan and Ravindran Balaraman. Transfer learning across heterogeneous robots with action sequence mapping. In *Proc. of the IEEE/RSJ International Conference on Intelligent Robots and Systems (IROS)*, pages 3251–3256, 2010.
- [10] Duy Nguyen-Tuong and Jan Peters. Model learning for robot control: a survey. *Cognitive processing*, 12(4):319–340, 2011.
- [11] Duy Nguyen-Tuong, Matthias Seeger, and Jan Peters. Model learning with local Gaussian process regression. *Advanced Robotics*, 23(15):2015–2034, 2009.
- [12] Chris J Ostafew, Angela P Schoellig, and Timothy D Barfoot. Learning-based non-linear model predictive control to improve vision-based mobile robot path-tracking in challenging outdoor environments. In *Proc. of the IEEE International Conference on Robotics and Automation (ICRA)*, pages 4029–4036, 2014.
- [13] Kaizad V Raimalwala, Bruce A Francis, and Angela P Schoellig. An upper bound on the error of alignment-based transfer learning between two linear, time-invariant, scalar systems. In *Proc. of the IEEE/RSJ International Conference on Intelligent Robots and Systems (IROS)*, 2015.
- [14] SB Russ. A translation of Bolzano’s paper on the intermediate value theorem. *Historia Mathematica*, 7(2):156–185, 1980.
- [15] Angela P Schoellig, Javier Alonso-Mora, and Raffaello D’Andrea. Limited benefit of joint estimation in multi-agent iterative learning. *Asian Journal of Control*, 14(3):613–623, 2012.
- [16] Angela P Schoellig, Fabian L Mueller, and Raffaello DAndrea. Optimization-based iterative learning for precise quadcopter trajectory tracking. *Autonomous Robots*, 33(1-2):103–127, 2012.

- [17] Sigurd Skogestad and Ian Postlethwaite. *Multivariable feedback control: analysis and design*, volume 2. Wiley New York, 2007.
- [18] Matthew E Taylor and Peter Stone. Transfer learning for reinforcement learning domains: A survey. *The Journal of Machine Learning Research*, 10:1633–1685, 2009.
- [19] Karl Tuyls and Gerhard Weiss. Multiagent learning: Basics, challenges, and prospects. *AI Magazine*, 33(3):41, 2012.
- [20] Chang Wang and Sridhar Mahadevan. Manifold alignment using procrustes analysis. In *Proc. of the 25th International Conference on Machine Learning*, pages 1120–1127, 2008.
- [21] Chang Wang and Sridhar Mahadevan. A general framework for manifold alignment. In *AAAI Fall Symposium on Manifold Learning and Its Applications*, pages 53–58, 2009.